Cell Reports

Article

# Single-cell transcriptomics identifies a WNT7A-FZD5 signaling axis that maintains fallopian tube stem cells in patient-derived organoids

## Graphical abstract

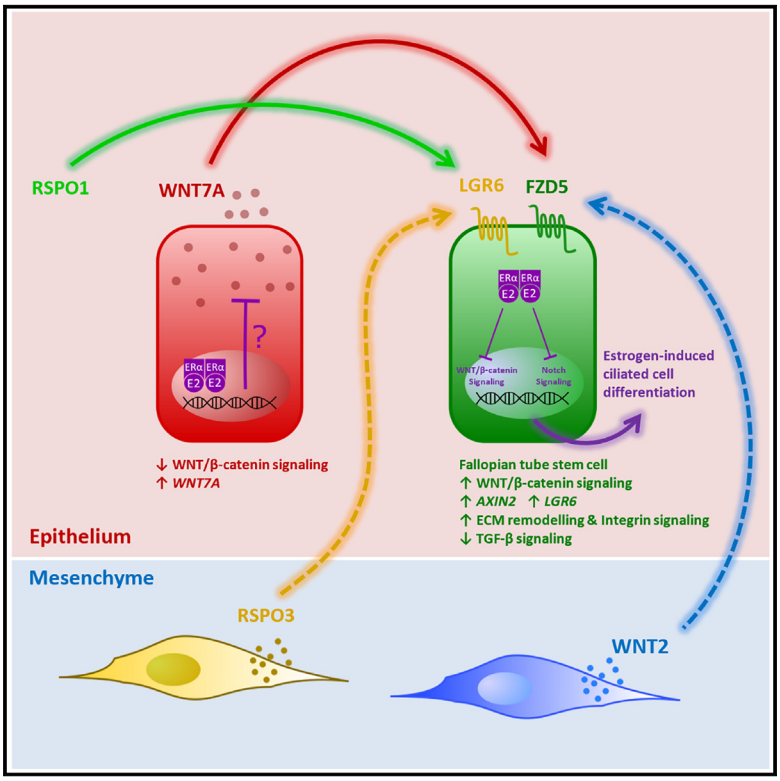


## Highlights

- Optimized conditions allow expansion of single FT cells into multi-lineage organoids
- WNT/β-catenin pathway reporter captures rare multipotent organoid-forming stem cells
- Fallopian tube (FT) stem cells are characterized with single-cell transcriptomics and mechanistic work
- An estrogen-regulated WNT7A-FZD5 signaling axis maintains FT stem cells

## Authors

Abdulkhaliq Alsaadi, Mara Artibani, Zhiyuan Hu, ..., Sachdev S. Sidhu, Joan S. Brugge, Ahmed Ashour Ahmed

## Correspondence

ahmed.ahmed@wrh.ox.ac.uk

## In brief

Progenitor fallopian tube cells are thought to initiate serous ovarian cancer, but their identification and characterization are lacking. Using optimized conditions to expand multi-lineage organoids from cells, Alsaadi et al. engineer reporter organoids to genetically tag, isolate, and characterize stem cells using mechanistic work and single-cell transcriptomics approaches.

Alsaadi et al., 2023, Cell Reports *42*, 113354
November 28, 2023 
https://doi.org/10.1016/j.celrep.2023.113354

CellPress

Cell Reports

CellPress
OPEN ACCESS

Article

# Single-cell transcriptomics identifies a WNT7A-FZD5 signaling axis that maintains fallopian tube stem cells in patient-derived organoids

Abdulkhaliq Alsaadi,[1,2,9] Mara Artibani,[1,2,3] Zhiyuan Hu,[1,2,3] Nina Wietek,[1,2,4] Matteo Morotti,[1,2,4] Laura Santana Gonzalez,[1,2] Moiad Alazzam,[4] Jason Jiang,[4] Beena Abdul,[4] Hooman Soleymani majd,[5] Levi L. Blazer,[6] Jarret Adams,[6] Francesca Silvestri,[7] Sachdev S. Sidhu,[6] Joan S. Brugge,[7,8] and Ahmed Ashour Ahmed[1,2,4,10,*]

[1]Ovarian Cancer Cell Laboratory, MRC Weatherall Institute of Molecular Medicine, University of Oxford, Oxford OX3 9DS, UK
[2]Nuffield Department of Women's & Reproductive Health, University of Oxford, Oxford OX3 9DU, UK
[3]Gene Regulatory Networks in Development and Disease Laboratory, MRC Weatherall Institute of Molecular Medicine, University of Oxford, Oxford OX3 9DS, UK
[4]Department of Gynecological Oncology, Churchill Hospital, Oxford University Hospitals, Oxford OX3 7LE, UK
[5]Medical Sciences Division, University of Oxford, John Radcliffe Hospital, Oxford OX3 9DU, UK
[6]School of Pharmacy, University of Waterloo, Waterloo, ON, Canada
[7]Department of Cell Biology, Harvard Medical School, Boston, MA 02115, USA
[8]Ludwig Center at Harvard, Boston, MA, USA
[9]Present address: Department of Cell Biology, Harvard Medical School, Boston, MA 02115, USA
[10]Lead contact
*Correspondence: ahmed.ahmed@wrh.ox.ac.uk
https://doi.org/10.1016/j.celrep.2023.113354

## SUMMARY

The study of fallopian tube (FT) function in health and disease has been hampered by limited knowledge of FT stem cells and lack of *in vitro* models of stem cell renewal and differentiation. Using optimized organoid culture conditions to address these limitations, we find that FT stem cell renewal is highly dependent on WNT/β-catenin signaling and engineer endogenous WNT/β-catenin signaling reporter organoids to biomark, isolate, and characterize these cells. Using functional approaches, as well as bulk and single-cell transcriptomics analyses, we show that an endogenous hormonally regulated WNT7A-FZD5 signaling axis is critical for stem cell renewal and that WNT/β-catenin pathway-activated cells form a distinct transcriptomic cluster of FT cells enriched in extracellular matrix (ECM) remodeling and integrin signaling pathways. Overall, we provide a deep characterization of FT stem cells and their molecular requirements for self-renewal, paving the way for mechanistic work investigating the role of stem cells in FT health and disease.

## INTRODUCTION

Despite their significance for fertility, reproduction, and women's health and disease, little is known about fallopian tube (FT) biology, cellular hierarchy, and homeostasis, which are critical for understanding infertility FT pathologies, including ectopic pregnancy, sexually transmitted infections, and FT-derived cancers. A number of studies have attempted to bridge this knowledge gap, showing that the distal human fallopian tube (hFT) and the distal region of its murine equivalent, the mouse oviduct (mOV), are enriched in stem-like cells possessing longevity and multipotency.[1–5] Studies in mice identified a population of label-retaining cells (LRCs) at the distal mOV[6] that are enhanced for differentiated spheroid formation.[3,4]

However, strong evidence of the existence of mOV stem cells came from *in vivo* lineage tracing that employed doxycycline-inducible labeling of secretory cells using a $Pax8^{rtTA}$ $TetO^{Cre}$ $YFP^{fl/fl}$ mouse model, demonstrating that ciliated cells emerge from secretory cells.[2] Similarly, in the hFT, putative stem cells have been shown to be secretory in nature, using spheroid,[7] air-liquid interface,[8] and organoid-based approaches.[9] Although this points to secretory cells as drivers of stem cell activity, we and others have recently uncovered a previously unappreciated heterogeneity within the FT secretory compartment,[10,11] using single-cell transcriptomics (SCT) profiling of fresh hFT tissue. Therefore, although *in vivo* and other studies refined the search for hFT/mOV stem cells, no studies have successfully pinpointed the secretory cell type driving FT renewal because of limitations in model tractability and difficulty in cell biomarking and isolation. Furthermore, humans and great apes possess FTs, whereas the equivalent in mice is the oviduct. Because of major anatomical differences, biological differences are likely to exist, and no studies have scrutinized whether mOV biology is representative of the hFT.

In addition to being a site where stem-like cells concentrate, as mentioned above, mounting evidence from several clinical and *in vivo* studies points to the distal FT fimbriae as the sites of origin of high-grade serous ovarian cancer [HGSOC].[12–14] HGSOC is a

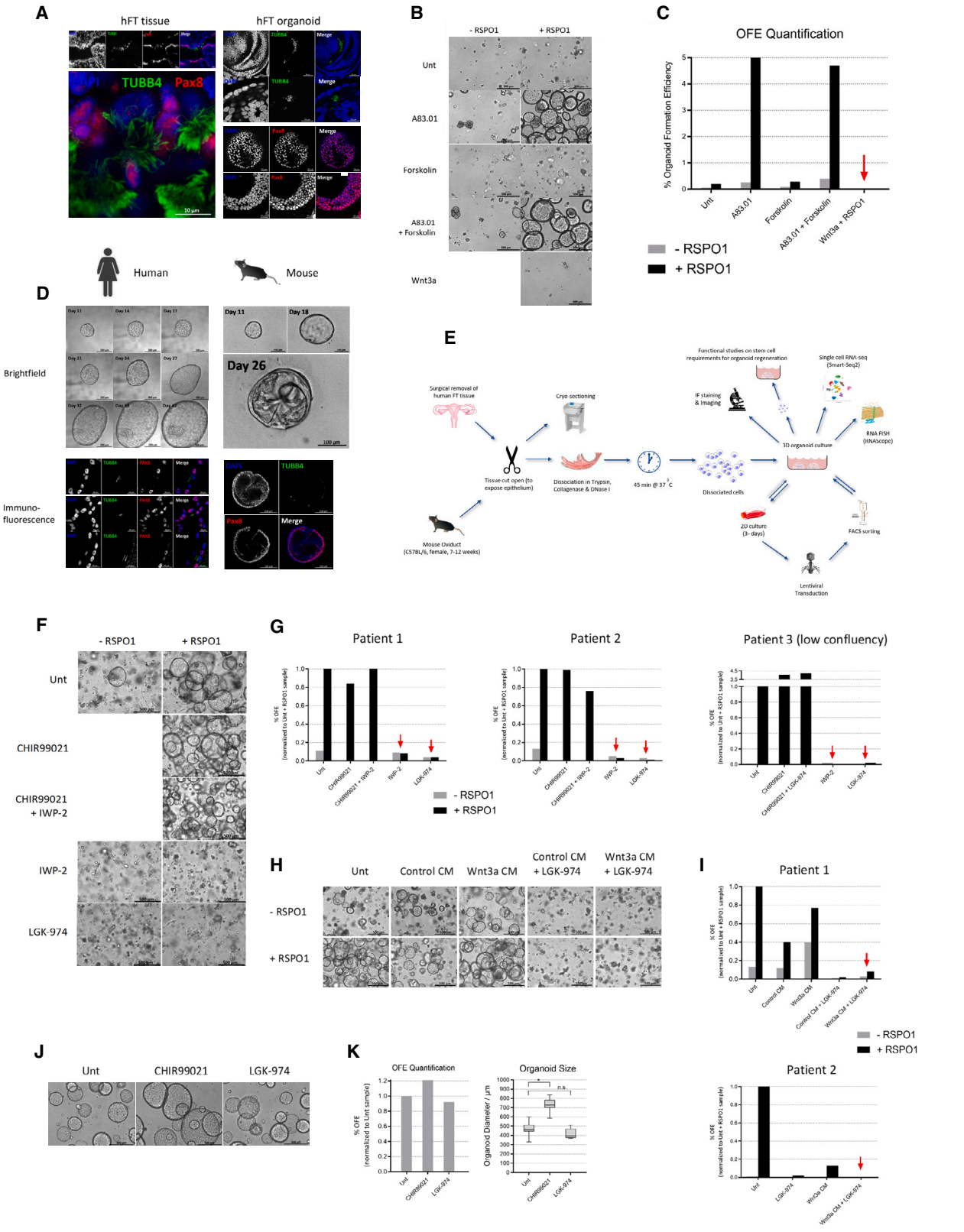


*(legend on next page)*

fatal gynecological malignancy with a dismal 5-year survival of 25% in late-stage disease.[15] The unusually specific localization of HGSOC precursor lesions to the distal FT is hypothesized to be due to proximity and regular exposure to ovulatory/follicular fluid, consistent with epidemiological studies reporting that natural (pregnancy or lactation) or artificial (oral contraceptive pills) pauses of ovulation have a protective effect against HGSOC, which was confirmed by the Million Women Study.[16] However, lineage-traced *Tp53* and *Brca1* mutant cells that initiate precursor lesions have been shown to be bipotent and arise preferentially from the distal oviduct in pre-pubertal mice that lacked ovulation, suggesting that FT/oviductal stem cells are strong candidates for being HGSOC cells of origin and that ovulation is not the sole determinant of the distal bias in FT/oviduct localization of HGSOC precursor lesions.[17] Therefore, understanding FT renewal may shed light on HGSOC initiation mechanisms, further reinforcing the urgency of this investigation. Here, we harness 3D patient-derived FT organoids to model FT regeneration *in vitro*. We genetically label, isolate, and characterize putative FT stem cells using functional approaches as well as bulk and SCT analyses, identifying a hormonally regulated WNT7A-FZD5 signaling axis that is critical for FT stem cell maintenance.

## RESULTS

### Optimizing robust regeneration of hFT organoids from single cells

Existing models of FT biology suffer from drawbacks that limit their utility in characterizing FT stem cells (Figure S1A). For example, conventional 2D cultures of primary FT cells (Figures S1B–S1D) lose epithelial markers within 5–6 weeks of culture (Figure S1E) and have been shown previously to lack ciliated cells.[10] In contrast, organoid cultures have been shown to be robust hFT/mOV models incorporating PAX8+ secretory and TUBB4+ ciliated cells,[3,9] and we reproduced this using the reported culture conditions (Figure 1A). However, a major limitation of human organoid culture is the lack of organoid regeneration after single-cell dissociation of patient tissue or organoids, a pre-requisite for isolating and characterizing putative stem cells. We reasoned that inhibitors contained within previously published culture conditions, including NOGGIN, which inhibits BMP-activated SMAD1/5/8-mediated signaling, and SB431542, an ALK4/5/7 inhibitor that blocks SMAD 2/3 transforming growth factor β (TGF-β)-mediated signaling, do not sufficiently inhibit TGF-β signaling to suppress differentiation and enable organoid regeneration. To address this, we employed another ALK4/5/7 inhibitor, A83.01, which has 10-fold higher potency compared with SB431542,[18] and found it to promote organoid formation efficiency (OFE) from single cells (Figures 1B, 1C, S2A, and S2B). Interestingly, we found that TGF-β suppression was not necessary for regeneration of mOV organoids from single cells (Figures S2C–S2E) and that it did not alter mOV size or OFE (data not shown).

In addition, we found that WNT3A conditioned medium (CM; Figure S3A) had no activity in hFT organoids and, indeed, reduced OFE (Figure S3B), most likely because of the presence of undefined serum factors. Using our optimized conditions containing A83.01/forskolin and lacking WNT3A, we verified that organoids emerge only from epithelial cells (Figure S3C), display invaginations characteristic of hFT tissue (Figure S3D), possess a spherical tube-like structure with a hollow interior (Video S1), and contain a rare population of KI-67+ proliferative cells (Figure S3E). We also confirmed that single cells dissociated into individual wells formed organoids containing PAX8+ and TUBB4+ differentiated progeny (Figure 1D), indicating that organoid regeneration is driven by multipotent stem cells. Overall, the data above indicate that the serum-free culture conditions we optimized robustly support the regeneration of hFT organoids from single stem cells. We set out to

**Figure 1. WNT/β-catenin signaling (WβS) is essential for organoid regeneration and is driven by unidentified endogenous WNT(s)**

(A) Confocal images of immunostaining for the secretory cell marker PAX8 and ciliated cell marker TUBB4 in fresh-frozen hFT sections or whole-mount immunostained hFT organoids. Organoids were grown for 10–13 days as described previously.[9] Representative of n = 3 patients. Scale bars are as indicated.

(B and C) The TGF-β inhibitor A83.01 restores OFE of single FT cells in an RSPO1-dependent manner.

(B) Representative bright-field images of EpCAM+ CD45− cells FACS isolated from patient tissue and organoid cultured for 12 days as indicated. Scale bar, 500 μm.

(C) Quantification of OFE for the samples shown in (B). A red arrow points to conditions of the reported method for culturing FT organoids. Representative of 2 biological replicates (n = 2 patients; second replicate, Figures S2A and S2B). Unt, untreated control.

(D) Representative images of organoids cultured from single FACS-isolated EpCAM+ CD45− cells derived from established organoid lines. Top: bright-field images taken on the indicated days. Bottom: representative confocal images of whole-mount immunostaining for differentiation markers.

(E) Graphical summary of the experimental approaches employed to biomark and characterize putative hFT/mOV stem cells.

(F and G) RSPO1 cooperates with endogenous WNT(s) to drive organoid regeneration.

(F) Representative bright-field images of passage 1 hFT organoids after 8 days of the treatments indicated. Scale bar, 500 μm.

(G) OFE quantification for the samples shown in (F) plus 2 additional patient replicates. 19,000, 12,000, or 7,000 cells were plated in 50-μL Matrigel drops on 24-well plates for patients 1, 2, and 3, respectively. Red arrows point to endogenous WNT secretion blockers abolishing OFE. (RSPO1) vs. (RSPO1 + IWP-2), $p = 0.0006$; (RSPO1) vs. (RSPO1 + LGK-974), $p < 0.0001$ (t test, two tailed, paired, n = 3 patient replicates). Four additional biological replicates (n = 4 patients) for the effect of endogenous WNT secretion blockers on OFE are shown later in a different context (Figures 4C and 4D).

(H and I) WNT3A does not rescue regeneration of WNT-blocked organoids.

(H) Representative bright-field images of hFT organoids after 8–9 days of the treatments shown. CM, conditioned medium. Scale bar, 500 μm.

(I) OFE quantification for the samples shown in (H) and another patient replicate. Red arrows point to WNT3A's failure to rescue endogenous WNT-blocked organoids. Activity of WNT3A CM was confirmed by the Wnt reporter (TOPFlash) assay (Figure S3A).

(J and K) Regeneration of mOV organoids is WβS independent.

(J) Representative bright-field images of mOV organoids after 11 days of the treatments shown (in the absence of RSPO1). Scale bar, 500 μm.

(K) Quantification of OFE (left) and organoid size (right) of samples shown in (J). OFE quantification (left) is representative of 5 biological replicates (2 replicates shown in Figures S2F and S2G, 2 replicates shown later in a different context; Figure 4G). Right: a boxplot for the sizes of the 10 largest organoids per sample. *$p < 0.0001$ (t test, two tailed).

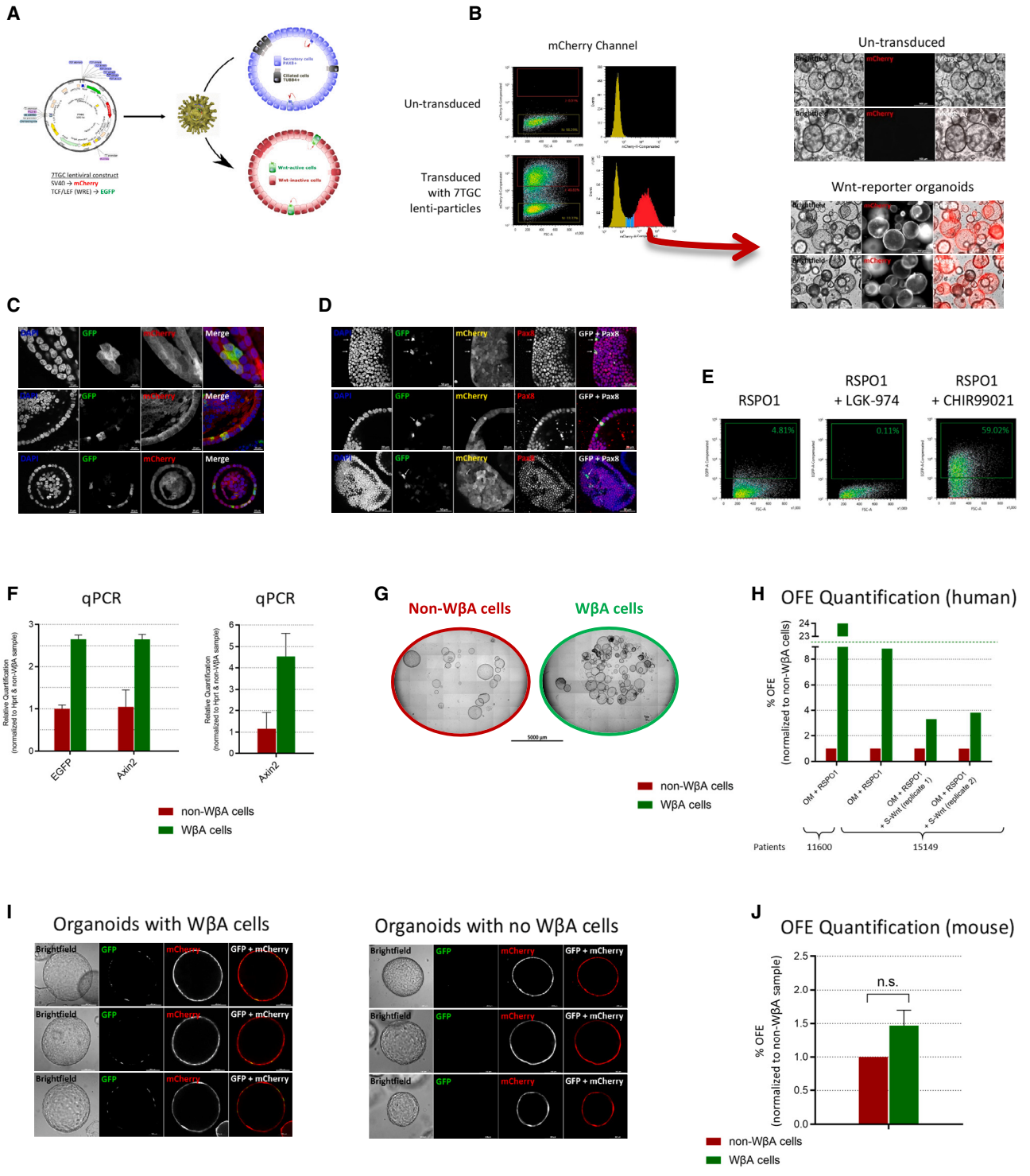


**Figure 2. WNT/β-catenin active (WβA) cells drive organoid regeneration**

(A) 7TGC lenti-construct used to generate WβS-reporter organoids (see STAR Methods for details).

(B) Left: FACS profile of mCherry expression upon viral transduction with 7TGC lenti-particles. Right: live-cell fluorescence microscopy images of 1-week-old organoids established from FACS-selected transduced cells (red arrow). Representative of 4 biological replicates (n = 4 patients). Scale bars, 500 μm.

*(legend continued on next page)*

characterize FT organoid-forming stem cells from multiple patients (Table S1) using several different approaches (Figure 1E).

## Wnt/β-catenin signaling is essential for renewal of hFT stem cells

WNT/β-catenin signaling (WβS) has been associated previously with hFT/mOV regeneration.[2,3,9] To investigate this further, we examined the effects of depletion or inhibition of multiple WβS pathway components on organoid regeneration. Withdrawal of RSPO1, which attenuates Wnt receptor turnover,[19,20] reduced OFE by more than 90% (Figures 1B and 1C), indicating that WβS is critical for stem cell renewal in organoids. To confirm this, we treated organoids with the tankyrase 1/2 inhibitor XAV-939[21] and the β-catenin/CBP inhibitor PRI-724,[22] which block WβS at midstream (cytoplasmic) and downstream (nuclear) nodes, respectively (Figure S3F). Both treatments completely abolished organoid regeneration (Figure S3G). Furthermore, in our optimized serum-free setting, RSPO1 is the only component that augments WβS (Figure S3H). Because our culture medium does not contain a WNT source, we reasoned that WβS is activated via an endogenously secreted WNT in organoids. Indeed, blocking endogenous WNT secretion using Porcupine inhibitors (Figure S3I) reduced OFE by over 90% (Figures 1F and 1G), phenocopying the effect of RSPO1 withdrawal (Figures 1B and 1C) and suggesting that RSPO1 cooperates with endogenous WNT to drive hFT organoid regeneration.

Contrary to the rescue of organoid regeneration seen in WNT-blocked intestinal organoids,[23] WNT3A failed to rescue the regeneration of WNT-blocked hFT organoids (Figures 1H and 1I), suggesting that it cannot substitute for the endogenously secreted WNT ligand. In contrast to hFT organoids, the regeneration of mOV organoids was unaffected by blocking endogenous WNTs (Figures 1J and 1K), suggesting that mouse organoids renew using WβS-independent mechanisms.

## WβS-active cells drive organoid regeneration

The results above indicate that WNT/β-catenin active (WβA) cells drive FT organoid regeneration. To isolate WβA cells, we transduced organoids from benign non-HGSOC patients with the WβS reporter 7TGC lentiviral vector[24] (Figure 2A), in which mCherry expression is driven by a constitutive (SV40) promoter, and EGFP expression is driven by TCF/LEF promoter elements, also called WβS-reporter elements (WβS-REs). We expanded fluorescence-activated cell sorting (FACS)-selected transduced cells using our optimized culture conditions to generate stable WβS-reporter organoids (Figures 2B and S4A) from multiple patients. Confocal imaging of fixed (Figure 2C) and live (Figure S4B) organoids confirmed localized activation of WβS. In addition, WβA cells were PAX8+/secretory in lineage (Figure 2D) and constituted 1.5%–5% of all cells (see Figures 2E and S4A for mOV and hFT organoids, respectively), mirroring the proportion of organoid-forming units in hFT organoids (Figure 1C). Blocking endogenous WNT secretion by LGK-974 treatment abolished EGFP+ cells (Figure 2E), while WβS activation using the GSK3 inhibitor CHIR99021 increased the proportion of EGFP+ cells over 10-fold (Figures 2E and S4C), suggesting that EGFP faithfully marked WβA cells. AXIN2, a reliable marker of WβS activation in several organoid systems,[25] including hFT organoids (Figure S4D), was elevated in EGFP+ cells (Figure 2F), further validating EGFP+ cells as WβA cells in this setting.

FACS-purified WβA cells displayed enhanced OFE relative to non-WβA cells (Figures 2G and 2H). While WβA cells were detected in all organoids within hFT organoid cultures, mOV organoids were either positive or negative for WβA cells (Figures 2I and S4F), and mOV WβA cells did not display enhanced OFE (Figure 2J) under a range of experimental conditions (Figures S4G–S4I), consistent with the WβS-independence seen in mOV organoids (Figures 1J and 1K).

## WNT7A is the driver of WβS and FT stem cell renewal

To identify the WNT ligand driving stem cell-mediated expansion of hFT organoids, we isolated WβA (EGFP+) and non-WβA (EGFP−) cells from WβS-reporter organoids and profiled their transcriptomes at the single-cell level. We applied the SMART-seq2 protocol[26] to a total of 1,021 cells (442 WβA cells and 579 non-WβA cells) from WβS-reporter organoids established from 3 patients. This identified *WNT7A* as the only robustly expressed WNT ligand in hFT organoids (Figure 3A). *WNT7A/Wnt7a* expression was further validated using RNAScope fluorescence *in situ* hybridization (FISH) staining in hFT organoids (Figure 3B; controls, Figure S5A), hFT tissue (Figures S5B and S5C), mOV organoids (Figure 3C; controls, Figure S5D), and mOV tissue (Figures S5E and S5F). We also found that *WNT7A+/Wnt7a+* cells were not exclusively positive or negative for the WβS activation markers *AXIN2* and *LGR5* (Figures 3B and 3C), so it remains unclear whether WNT7A signals in an autocrine or paracrine manner. However, our single-cell RNA sequencing (scRNA-seq) data implicate WNT7A as the target of the Porcupine inhibitors IWP-2 and LGK-974, which abolish organoid regeneration (Figures 1F–1I). In contrast, *WNT3A* expression

(C and D) Confocal imaging of fixed, whole-mounted hFT WβS-reporter organoids showing WβA (EGFP+) cells (C) and their secretory (PAX8+) lineage, shown by white arrows (D). Representative of 4 biological replicates (n = 4 patients). Scale bars are as indicated.
(E) FACS analysis of EGFP expression in mOV WβS-reporter organoids treated for 13 days as indicated. Representative of 5 biological replicates (two replicates shown later in other contexts: Figures 4B and S4C).
(F) Representative qRT-PCR analysis of the relative mRNA expression of EGFP and the WβS activation marker Axin2 in WβA vs. non-WβA cells that were FACS isolated from mOV WβS-reporter organoids. Error bars represent mean ± 95% confidence interval for three technical replicates. Right: a second biological replicate.
(G and H) hFT WβA cells are enriched in organoid formation ability.
(G) Representative brightfield whole-well images of organoids formed by WβA or non-WβA cells after FACS isolation and organoid culture for 22 days. 25,000 cells were plated in 50-μL Matrigel drops on 24-well plates. Scale bar, 5,000 μm.
(H) Quantification of OFE enrichment in WβA cells, shown for 2 patients and under different treatment conditions for 1 patient. WβA and non-WβA cells for the same 2 patients (and others) were further analyzed by scRNA-seq analysis (shown later; Figure 6).
(I) Live-cell imaging of mOV WβS-reporter organoids after 1–2 weeks in culture. Images are representative of more than 100 organoids. Scale bars, 500 μm.
(J) Quantification of OFE in mOV WβA vs. non-WβA cells. Error bars represent mean ± SEM for 5 biological replicates. n.s., not significant.

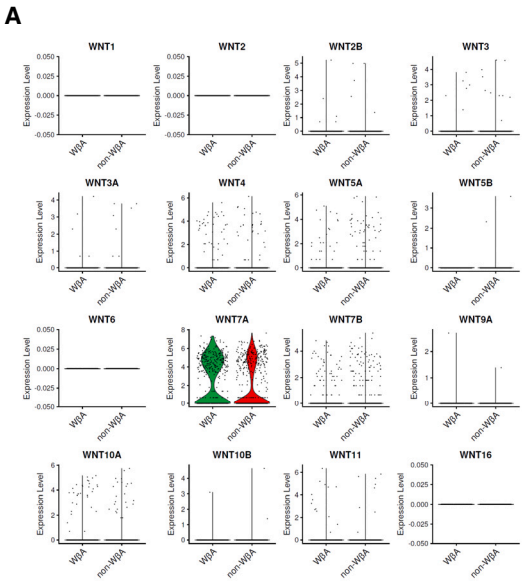


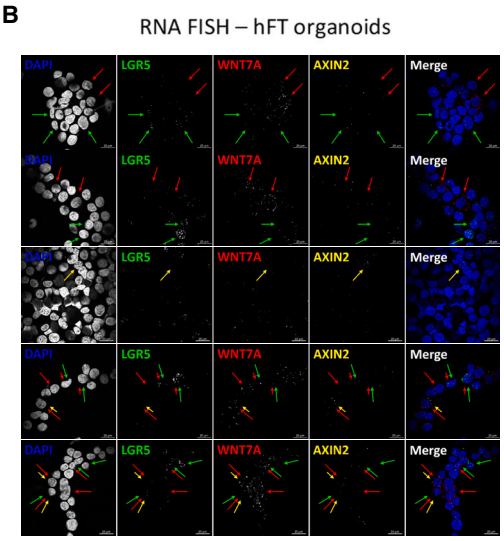


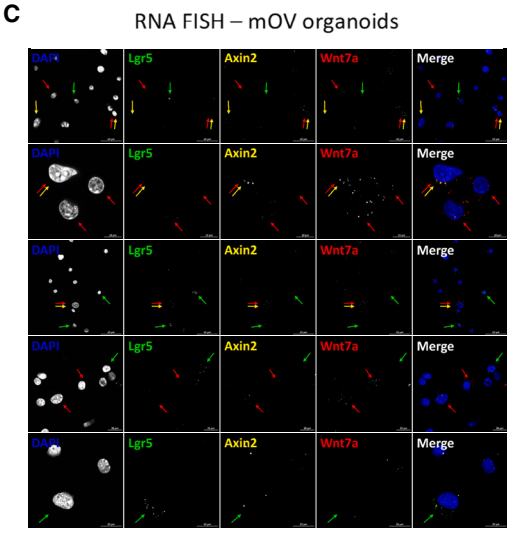


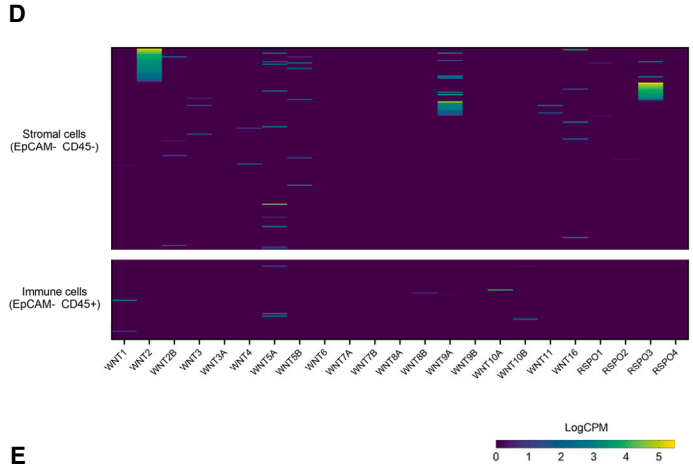


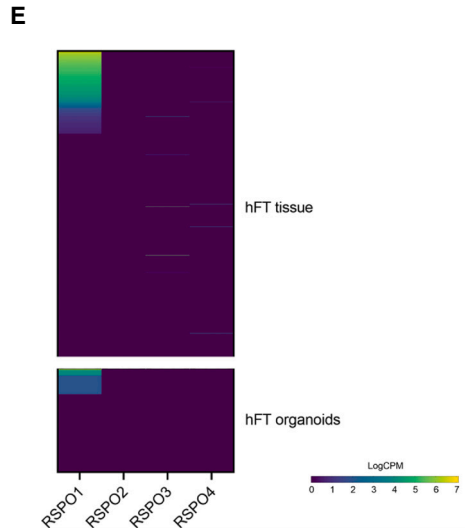


*(legend on next page)*

was not detected in organoids (Figure 3A), suggesting that hFT cells are not naturally primed to respond to WNT3A or activate WβS through it. This is consistent with WNT3A's failure to rescue growth of WNT-blocked organoids (Figures 1H and 1I).

Next, we surveyed the expression of the WNT family of ligands in our previously published SCT dataset from stromal and immune cells isolated from patient tissue.[10] This analysis showed that 25% of stromal cells express *WNT2* and 7.5% express *WNT9A* (Figure 3D), suggesting that epithelial WNT7A may be redundant for FT renewal *in vivo*. Furthermore, because endogenous RSPO1, the predominant R-Spondin family ligand expressed in hFT tissue and organoids (Figure 3E), is not sufficient to promote organoid regeneration, we reasoned that another source of RSPOs could be involved *in vivo*. Our non-epithelial SCT dataset showed that 10% of stromal cells robustly express *RSPO3* (Figure 3D), which biochemical studies indicate is over 20-fold more potent in augmenting WβS compared with RSPO1.[27] Notably, the *WNT2*+, *WNT9A*+, and *RSPO3*+ stromal cells are largely distinct, and we do not see a robust WNT or R-Spondin contribution from the limited number of immune cells profiled (Figure 3D).

Next, we sought to functionally confirm whether WNT7A is essential for renewal of FT stem cells in organoids. Ten lentiviral shRNA vectors from two commercial sources were tested by FACS-isolating and expanding stably transduced SKOV3 cells, a cell line we previously confirmed to express high levels of WNT7A. Our qPCR and western blot data indicated that the constructs were not effective in knocking down *WNT7A*/WNT7A levels (data not shown). We also aimed to test whether WNT7A protein rescues OFE of WNT-blocked organoids. In line with the reported difficulties in generating functional WNTs for *in vitro* assays,[28] all generated WNT7A protein reagents were not functional, including WNT7A CM derived from *WNT7A* cDNA plasmid-transfected HEK293 cells (Figures S6A and S6B); WNT7A CM from primary 2D-cultured FT cells (Figure S6C), which we find to endogenously overexpress WNT7A (Figures S6D and S6E); native WNT7A protein (Figure S6F); and recombinant WNT7A protein from two commercial sources (one shown in Figure S6G). Interestingly, the *WNT7A* cDNA expression plasmid robustly activated WβS in the TOPFlash assay, but the CM derived from the same cDNA plasmid-transfected cells failed to activate WβS (Figure S6G) despite containing abundant WNT7A protein (Figures S6A and S6B). We reasoned that this could be due to a short signaling range, which has been shown by biochemical and *in vivo* approaches for certain WNT ligands.[29–31] We confirmed this for WNT7A using a simple co-culture assay (Figures S6H and S6I), which explained why our protein-based WNT7A reagents were not functional.

Finally, we confirmed the observation above, the ability of WNTs to activate WβS as transfected cDNA plasmids but not as secreted proteins derived from the same plasmid, for 4 other canonical WNTs (data not shown). In contrast, we found WNT3A deviates from this pattern in that it robustly activates WβS as a transfected cDNA plasmid and as a secreted protein derived from the same plasmid as the above WNTs (Figure S6J), implying a unique functional or signaling biology that merits further investigation.

## FZD5 mediates WNT7A-driven maintenance of FT stem cells

To overcome the above limitations and test the functional contribution of WNT7A to organoid renewal, we attempted to identify and biochemically perturb the WNT7A receptor in organoids. SCT profiling identified *FZD3*, *FZD5*, *FZD6*, and *FZD10* as the major Frizzled (FZD) receptors expressed in hFT organoids (Figure 4A). Excluding *FZD10*, these were also the major FZDs expressed in hFT tissue (Figure S7A). The FZD3/6 subfamily is the most divergent from other FZD family members (Figure S7B) and participates in non-canonical WNT signaling.[32] FZD5, but not FZDs 3/6/10, has been reported to bind WNT7A and activate WβS, as shown in *in vitro* WNT-FZD pair screens[33,34] and *in vitro* models.[35,36] Based on these reports, we ruled out FZD10 as a receptor that transduces WNT7A-induced WβS in hFT organoids. Furthermore, to validate the findings of previous reports, we utilized HEK293 cells, which endogenously express FZDs 3/5/6 (Figure S7C). Small interfering RNA (siRNA) knockdown (Figure S7D) of *FZD5*, but not *FZD3* or *FZD6*, inhibited *WNT7A*-induced TOPFlash (Figure S7E), while WNT7A induced the highest WβS/TOPFlash signal in a background of FZD5 overexpression compared with FZD3 or FZD6 overexpression (Figure S7F).

Although these data confirm that WNT7A can activate WβS through FZD5, direct functional evidence from hFT organoids is lacking. To address this, we utilized immunoglobulin G (IgG)-2919 and IgG-2921, two selective, antibody-based inhibitors of FZD5 generated using an antibody phage display system.[37] Anti-FZD5 IgGs reduce the TOPFlash signal in WNT7A- and FZD5-overexpressing cells by more than 60% (Figure S7G). Consistent with the dual effect of WNT inhibition on abolishing WβA cells (Figure 2E) and OFE (Figures 1F–1I), FZD5 inhibition abolished WβA cells (Figure 4B) and OFE (Figure 4C) by over 90% (Figure 4D). This phenocopies the effect of RSPO1 withdrawal (Figures 1B, 1C, and 1F–1I). The only other FZD that shows cross-reactivity with anti-FZD5 antibodies is FZD8 (Figures 3C; Figure S5 in Steinhart et al.[37]), which is not expressed in hFT organoids (Figure 4A). Furthermore,

**Figure 3. WNT7A is the WNT ligand that cooperates with RSPO1 to drive WβS and organoid regeneration**

(A) Violin plots showing the scRNA-seq profile of the WNT family of ligands in WβA (GFP+) and non-WβA (GFP−) cells FACS isolated from WβS-reporter organoids (n = 3 patients). Each dot represents one cell. Based on SCT data, the frequency of WNT7A+ cells is ~5% in hFT tissue and ~20% in hFT organoids.

(B and C) Confocal images of RNAScope FISH staining for the WNT7A/Wnt7a and WβS activation markers AXIN2/Axin2 and LGR5/Lgr5 in hFT (B) and mOV (C) organoids. Arrows point to cells expressing color-matched genes. Arrow clusters indicate co-expression. LGR5+/Lgr5+ cells and AXIN2+/Axin2+ cells are largely distinct. Organoids were dissociated, cytospun, and fixed prior to RNA FISH staining. Scale bars are as indicated.

(D) Heatmap showing the scRNA-seq profile of the WNT and R-Spondin family of ligands in the non-epithelial compartments of hFT tissue. Stromal (n = 6 patients) and immune (n = 1 patient) cells were FACS isolated using the antibodies indicated. Each row represents one cell. scRNA-seq was performed according to the SMART-seq2 protocol[26] and as described previously.[10]

(E) Heatmap showing the scRNA-seq profile of the R-Spondin family of proteins in epithelial hFT tissue (top) and hFT organoids (bottom). Each row represents one cell.

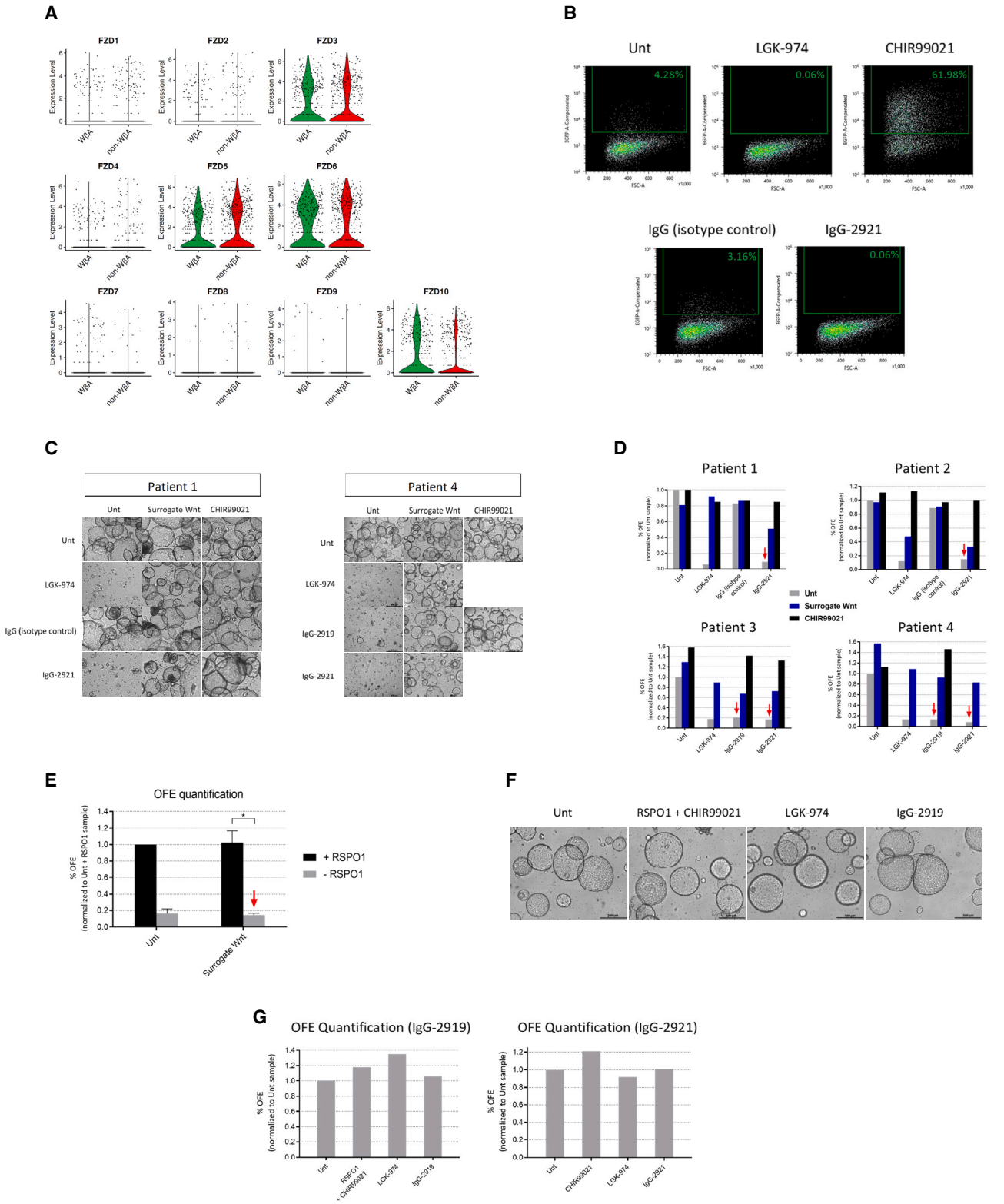


**Figure 4. FZD5 is the WNT7A receptor**

(A) Violin plots showing the scRNA-seq profile of the Frizzled family of receptors in WβA (GFP+) and non-WβA (GFP−) cells FACS isolated from WβS-reporter organoids (n = 3 patients). Each dot represents one cell.

*(legend continued on next page)*

FZD5-inhibited or WNT-blocked organoids were rescued by WβS activation downstream of ligand-receptor interactions using the selective GSK-3β inhibitor CHIR99021 (Figures 4C and 4D). Partial rescue is also observed when WβS is activated at the ligand-receptor level using surrogate Wnt (Figures 4C and 4D), which competes with anti-FZD5 IgGs for binding to FZD's cysteine-rich domain.[37,38] Surrogate Wnt has broad-spectrum activity against FZD1/2/5/7/8 but not FZD3/6/10.[38] Because only FZD3/5/6/10 are expressed in hFT tissue and organoids, this provides further evidence that FZD5 is the FZD receptor associated with WβS and organoid regeneration. FZD receptors are subject to constant turnover and proteasomal degradation by the action of the RNF43/ZNRF3 ubiquitin ligases,[19] which are inhibited by R-Spondins.[39–41] Therefore, withdrawal of RSPO1 from surrogate Wnt-treated organoids reduces OFE by 75%–90% (Figure 4E). Because FZD5 is the only FZD targetable by surrogate Wnt, this indicates that the reduced OFE seen upon RSPO1 withdrawal from surrogate Wnt treated (Figure 4E) and untreated (Figures 1B, 1C, and 1F–1I) organoids is due to FZD5 turnover. Altogether, these data strongly suggest that FZD5 is the cognate receptor for endogenous WNT7A in the FT and that a WNT7A-FZD5 signaling axis drives WβS activation and renewal of hFT organoids.

While organoids from tested patients in this study showed sensitivity to WβS inhibition, organoids from one patient were resistant to WNT and FZD5 inhibition (Figures S8A and S8B) as well as to RSPO1 withdrawal (Figure S8C). Patient 5 organoids were, however, sensitive to downstream WβS inhibition using XAV-939 and PRI-724 (Figures S8A and S8B), as seen in other patients (Figure S3G). Tested under selective conditions of WNT blocking for four passages, patient 5 organoids showed ectopic and robust growth that led to large organoid sizes not typical for normal FT organoids (Figure S8D). Although patient 5 was diagnosed with serous ovarian cancer, which is thought to derive from the FTs,[13,14] patient 5 organoids did not carry TP53 mutations, which are known to be early events in HGSOC.[12] In light of studies showing niche independence of organoids from tumor samples[42,43] or normal organoids engineered by CRISPR-Cas9 methods to harbor tumorigenic mutations,[44,45] it is tempting to speculate that these WNT/FZD5-resistant organoids may represent mutant clones with early somatic, copy number, or epigenetic (chromatin-associated or DNA methylation) changes that confer a selective growth advantage and independence from stem cell niche factors. Further genomic and functional characterization as well as more patient replicates are required to conclusively establish this.

Finally, FZD5 inhibition has no effect on mOV organoids (Figures 4F and 4G), consistent with the lack of effect seen upon blocking WNT secretion (Figures 1J and 1K) and lack of OFE enrichment in isolated WβA mOV cells (Figure 2J). This is despite WNT blocking and FZD5 inhibition abolishing WβA cells in mOV WβS-reporter organoids (Figure 4B), suggesting that a WNT-FZD5 signaling axis also regulates WβS in mOV organoids, but unlike in hFT organoids, WβS is not essential for stem cell renewal in the mOV organoids.

## Estrogen downregulates WNT7A and triggers differentiation

Female reproductive tract (FRT) organs, including the hFT/mOV, are subject to cyclic hormonal influences. Studies indicate that estrogen activates WβS in the FRT,[46–48] while other reports provide evidence that estrogen exerts an inhibitory influence on WNT7A.[49–51] To address this knowledge gap, we examined the effects of estrogen on WNT7A and WβS in our FT organoid model.

Our SCT data confirm that our optimized organoid culture conditions successfully maintain hormone receptor-expressing cells (Figure 5A), as seen in human tissue (Figure 5B). In both settings, estrogen receptor $\alpha$ (ER$\alpha$) is the predominant hormone receptor expressed, and we harnessed this model to understand estrogen's influence on the FTs. Estrogen treatment of hFT organoids triggers a phenotype of organoids with shriveled, condensed, and darker morphology with extensive internal folding and invaginations (Figures 5C and 5D, left) without significantly impairing OFE (Figure 5D, right). This morphology is reminiscent of the differentiation morphology that appeared in long-term cultured organoids (Figure 1D) and upon inducing differentiation conditions in organoids of other tissues.[52–54] However, estrogen triggered these changes within 72 h. On the molecular level, hFT organoids respond robustly to estrogen treatment by upregulating the expression of the canonical estrogen target genes *PGR* and *TFF1* (Figure 5E), and in this setting, we found that estrogen downregulated expression of *WNT7A* and the RSPO1 receptor *LGR6* as well as the WβS reporter *AXIN2* (Figure 5F). Furthermore, we detected downregulation of the secretory cell marker *PAX8* and upregulation of *FOXJ1* (Figure 5G), an established master regulator and marker of ciliated cells,[55] as well as upregulation of *CAPS*, *CCDC17* (Figure 5G), and *CCDC78* (Figure 5H), all ciliated cell markers we identified previously in a tissue-based SCT study.[10] Progesterone did not antagonize estrogenic molecular changes in this setting (Figures 5E–5G). Therefore, estrogen triggers hFT organoid differentiation toward the ciliated cell lineage.

(B) FACS analysis of EGFP expression in mOV WβS-reporter organoids upon treatment with anti-FZD5 (IgG-2921) antibody for 7 days. Green gates within plots indicate the percentage of EGFP+ cells.
(C and D) FZD5 mediates WβS-dependent regeneration of hFT organoids.
(C) Representative bright-field images of passage1 hFT organoids treated for 10–13 days as indicated. Images for two biological replicates (n = 2 patients) are shown. All samples contained RSPO1. Scale bars, 500 μm.
(D) OFE quantification for samples shown in (C) plus 2 additional patient replicates. Red arrows point to OFE reduction by anti-FZD5 antibodies. Unt vs. LGK-974, $p < 0.0001$ (n = 4 patients); Unt vs. IgG-2921, $p < 0.0001$ (n = 4 patients). The p values were calculated using Student's t-test, two tailed, paired.
(E) Quantification of reduction in surrogate Wnt-driven OFE upon RSPO1 withdrawal (red arrow). Error bars represent mean ± SEM for three biological replicates (n = 3 patients). *p = 0.0036 (t test, two tailed).
(F and G) mOV OFE is unaffected by blocking the FZD5 receptor.
(F) Representative bright-field images of mOV organoids treated for 11 days as indicated (in the absence of RSPO1, unless otherwise indicated). Scale bars, 500 μm.
(G) Quantification of OFE for the samples shown in the left panel of (F) and another biological replicate using a different anti-FZD5 IgG (IgG-2921, right).

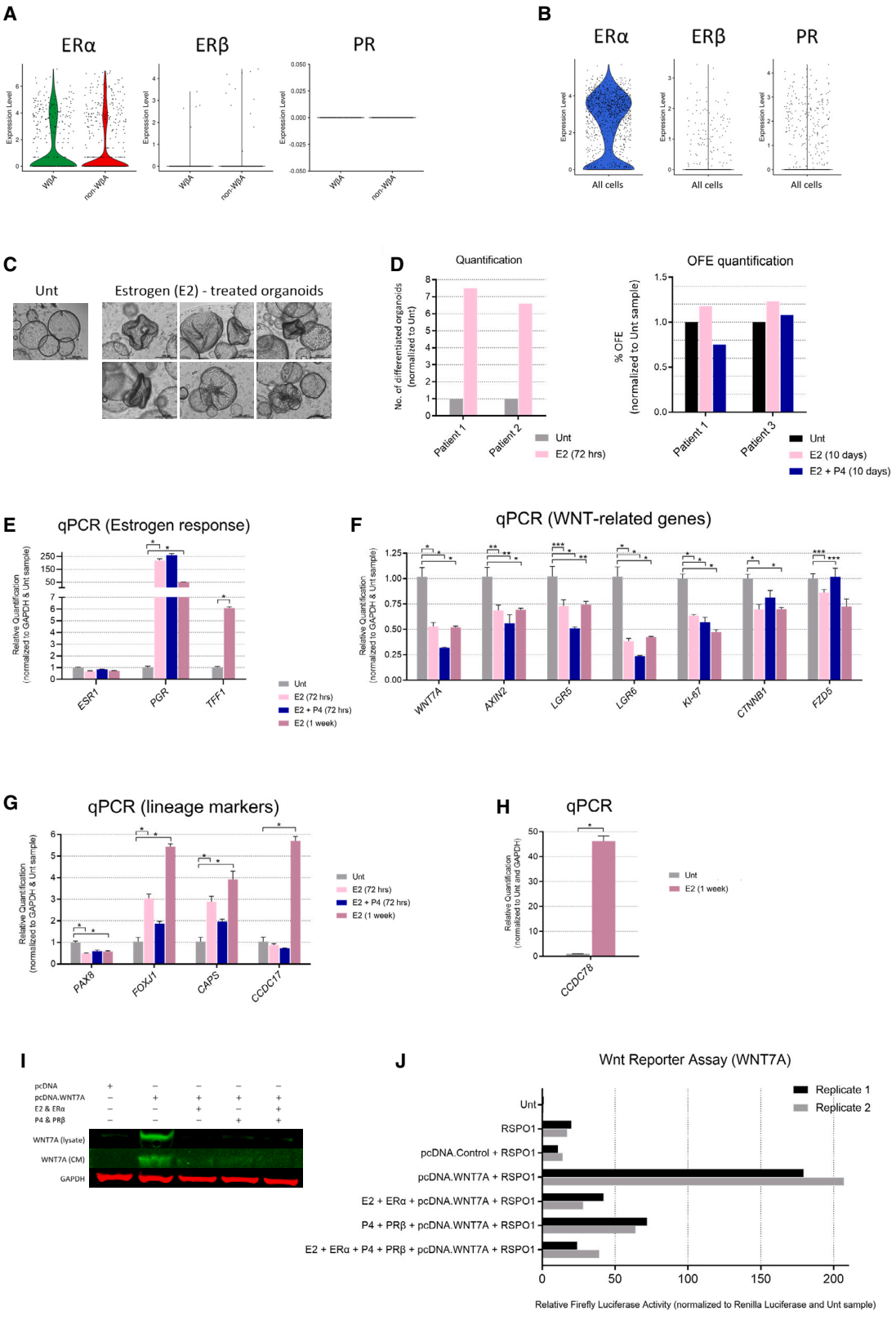


*(legend on next page)*

Inhibition of the Notch signaling pathway has been reported to promote the ciliated cell lineage in hFT/mOV organoids.[3,9] To determine whether estrogen induces ciliogenesis through inhibiting Notch signaling, we treated hFT organoids with the Notch signaling inhibitor DAPT, which reduced the expression of Notch target genes (Figure S9A). In addition to downregulating WNT7A and WβS, estrogen downregulated the expression of Notch target genes to levels comparable with the Notch inhibitor DAPT (Figures S9A). However, unlike estrogen treatment, inhibition of Notch signaling alone did not potently induce ciliogenesis in hFT organoids (Figures S9C and S9D). We next asked whether estrogen's influence could be phenocopied by inhibiting WβS and Notch signaling. To this end, we found that treatment of organoids with small-molecule inhibitors of endogenous WβS (LGK-974) and endogenous Notch signaling (DAPT) phenocopied the ciliogenesis-inducing effect triggered by estrogen (Figures S9C and S9D), suggesting that estrogen influences cell fate decisions in hFT organoids, at least in part, through downregulating the WNT and Notch pathways.

To further examine the effects of estrogen and progesterone on WβS, we directly examined the influence of these hormones on transcription at the WβS-REs using the TOPFlash assay in HEK293 cells. Estrogen robustly activated transcription from WβS-RE (Figure S9E), independent of WNT ligands (Figure S9F). Estrogen's activation of transcription at WβS-REs was unaffected by WβS inhibitors at midstream (XAV-939) and downstream (PRI-724) levels (Figure S9F). Estrogen also attenuated ligand-dependent and ligand-independent hyperactivation of WβS (Figure S9G) to levels seen in estrogen-treated samples (Figure S9E), indicating that liganded estrogen-ERα complex may compete with β-catenin for binding and activation at WβS-REs. To test this hypothesis, we investigated the effect of estrogen on TOPFlash signal upon β-catenin knockdown. β-Catenin siRNAs were validated to effectively abolish β-catenin protein levels (Figure S9H) and activity (Figures S9I and S9J). In this setting, liganded ERα activated transcription at WβS-REs independent of β-catenin (Figure S9K) and induced WβS target gene transcription 45%–88% higher in the absence of β-catenin, suggesting that the pair competes for binding at WβS-RE promoter elements. Next, we sought to delineate the effect of estrogen on WNT7A. Interestingly, estrogen (as well as progesterone) dramatically reduced intracellular and secreted WNT7A protein levels (Figure 5I) and activity (Figure 5J) without independently activating WβS (Figure S9E). Overall, these data suggest that estrogen can activate WβS target gene expression in ERα-expressing hormone-responsive tissues, but in the presence of WNT7A (exogenously expressed in HEK293 cells and endogenously present in FT organoids), estrogen specifically suppresses WNT7A and WNT7A-induced WβS.

Finally, WβS inhibition has been shown recently to downregulate the expression of DNA double-strand break repair genes, including *BRCA1*, *BRCA2*, *RAD51*, and the *FANC* gene family, in various tissues via a WβS-MYBL2 signaling axis.[56,57] These DNA repair genes have been shown to be upregulated endogenously in WβA cells of other tissues.[56] In addition to inhibiting WβS, we noted that estrogen suppresses *MYBL2* as well as *BRCA1* and *BRCA2* expression in hFT organoids (Figure S9L). This is phenocopied by estrogen-independent WNT inhibition (Figure S9L), raising the possibility that estrogen may regulate *MYBL2* and *BRCA1/2* expression, at least in part, through regulating WβS.

Collectively, the data presented above indicate that estrogen suppresses *WNT7A* and WβS, robustly induces a transcriptional ciliogenesis program, and may regulate *BRCA1/2* expression in hFT organoids.

## Transcriptomic characterization of WβA cells

Our data so far reveal a hormonally regulated WNT7A-FZD5 signaling axis that activates WβA cells that drive hFT organoid regeneration, identifying WβA cells as candidate FT stem cells. To further characterize these cells, we performed scRNA-seq (SMART-seq2 protocol[26]) on 442 WβA and 579 non-WβA cells isolated from WβS-reporter organoids established from three patients. Unsupervised clustering using uniform manifold approximation and projection (UMAP) showed that WβA cells are enriched in specific clusters of cells that are distinct from non-WβA cells (Figure 6A). To identify the genes responsible for driving this difference, we conducted an intra-patient differential gene expression analysis between WβA and non-WβA cells, identifying expression signatures that are enriched in these cell types (Figure 6B; raw data containing full gene lists are

**Figure 5. Estrogen suppresses WNT7A and WβS and promotes differentiation of hFT organoids**

(A and B) Violin plots showing the scRNA-seq profile of female hormone receptors in hFT organoids (A) and hFT tissue (B).

(A) Data from WβA (GFP+) and non-WβA (GFP−) cells FACS isolated from WβS-reporter organoids (n = 3 patients).

(B) Data from EpCAM+ CD45− cells FACS isolated from hFT tissue.[10] Each dot represents one cell.

(C and D) Estrogen triggers ciliated cell differentiation in hFT organoids.

(C) Representative bright-field images of differentiated organoids that arise after treatment with estrogen (17β-estradiol, 100 nM) for 72 h. Scale bar, 500 μm.

(D) Left: quantification of enrichment in differentiated organoids shown in (C) plus another replicate. Right: OFE quantification of organoids treated with E2 (17β-estradiol, 100 nM) with or without P4 (progesterone, 1 μM) for 10 days. All samples contained RSPO1. Quantification is shown for 2 replicates (n = 2 patients). Patient 1 organoids on the left and right are the same patient.

(E–H) Estrogen suppresses WNT7A and WβS to induce ciliogenesis in hFT organoids. Shown is qRT-PCR analysis of the relative mRNA expression of (E) ESR1 and the canonical ER target genes PGR and TFF1; (F) WNT7A, AXIN2, LGR6, and other WNT-related genes; and (G and H) secretory and ciliated cell markers. For (E–H), treatments were administered to expanded organoids 7–9 days after initial plating. Estrogen (17β-estradiol, 100 nM) or progesterone (1 μM) was administered at the indicated concentrations for 72 h (short term) or 1 week (long term) as indicated. Data in (E–H) are for the same samples. E2 (1 week) treatment is normalized to the Unt (1 week) control sample (not shown for simplicity). Error bars represent mean ± SEM for 3–6 technical replicates. Asterisks denote statistical significance, calculated using unpaired Student's t-test, as follows: (E) *p < 0.00008, (F) *p < 0.009, **p < 0.05, ***p = n.s.; (G) *p < 0.004, (H) *p < 0.0001. Additional replicates (3–12 technical replicates, n = 2 patients) for the effect of estrogen on the indicated genes are shown in Figures S9A–S9D in a different context.

(I–J) Estrogen (and progesterone) downregulate WNT7A protein level (I) and activity (J).

(I) Western blot showing cytoplasmic (lysate) and secreted (CM) levels of WNT7A protein. Representative of n = 2 biological replicates.

(J) TOPFlash assay with the indicated treatments. All samples were transfected with the pcDNA.WNT7A construct and treated with RSPO1.

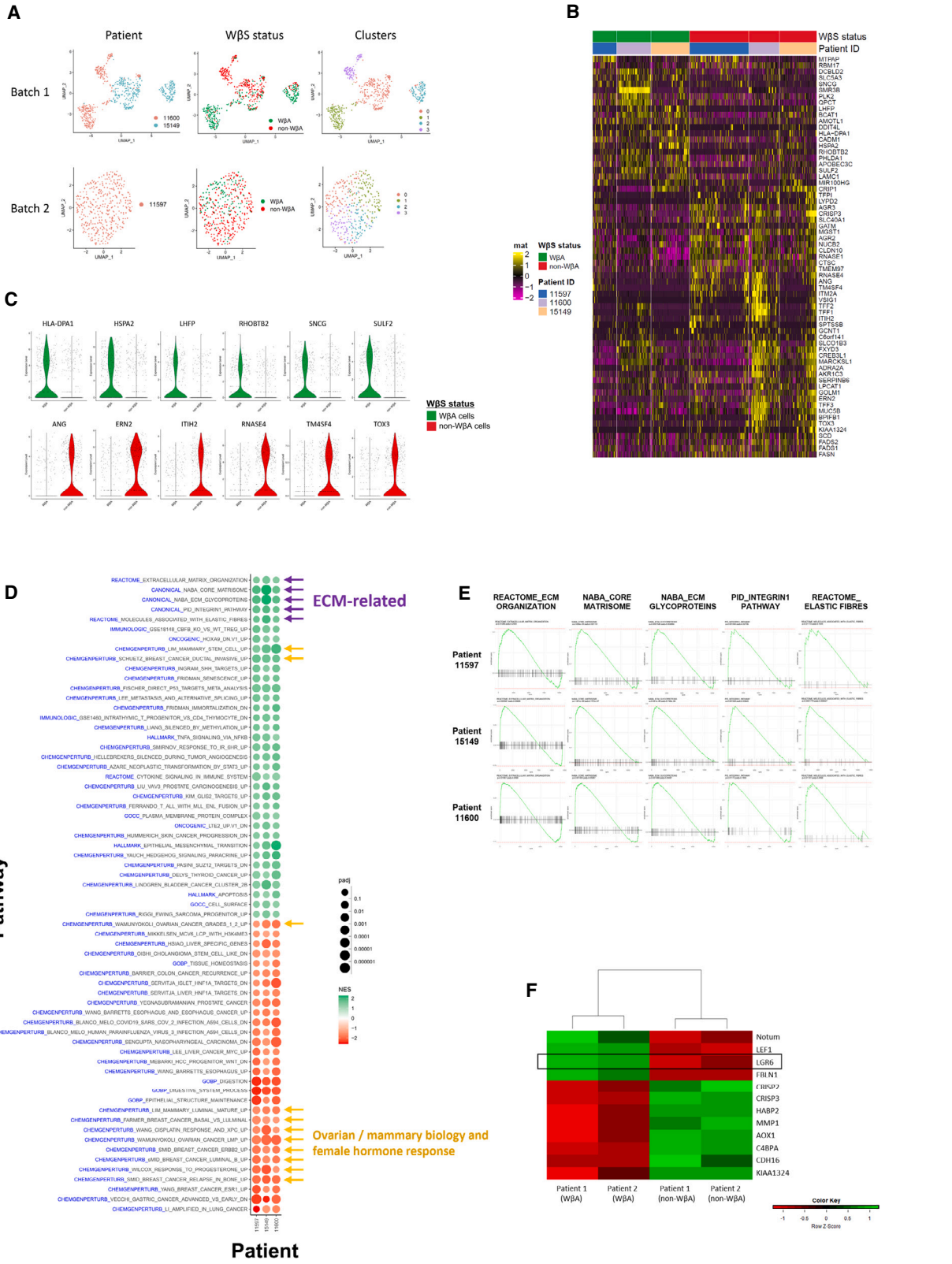


*(legend on next page)*

provided in Table S2). Among these we noted a small number of specific or highly differentially expressed genes that could potentially serve as biomarkers for future studies focusing on gene-based identification or isolation of WβA cells (Figure 6C).

To further explore the nature of pathways and processes that characterize WβA cells, we conducted gene set enrichment analyses (GSEAs) based on our scRNA-seq data (raw data of the full gene set lists are provided in Table S3). Several WβS-related pathways and processes were enriched in WβA cells (Table S3), validating our strategy for capturing WβA cells using WβS-reporter organoids. WβA cells were also enriched in pathways associated with female hormone responsiveness as well as ovarian and mammary tissue biology and cancer (Figure 6D), consistent with the tissue of origin of our reporter organoid lines. The most common WβA cell-enriched gene sets, however, are associated with extracellular matrix (ECM) remodeling and integrin signaling in patient-shared (Figures 6D and 6E) and patient-unique (Table S3) analyses, suggesting that ECM processes may play a dominant role in maintaining WβA cells.

Finally, we probed the scRNA-seq dataset to identify the RSPO1 receptor responsible for the obligate RSPO1 requirement in hFT organoid regeneration (Figures 1B, 1C, and 1F–1I). We found that our organoid SCT data do not capture the expression of R-Spondin receptors (LGR4–LGR6), possibly because of dropout of low-abundance mRNAs. To address this, we performed bulk RNA-seq of WβA and non-WβA cells that were FACS isolated from WβS-reporter organoids. Similar to the SCT organoid data, the bulk RNA-seq data confirmed enrichment of WβS-related processes and pathways in WβA cells (Table S4) and identified *LGR6* as the only R-Spondin receptor enriched in WβA cells (Figure 6F). This is consistent with our previous functional data, in which organoid differentiation-inducing conditions significantly reduce the expression levels of the WβS reporter gene *AXIN2* concomitant with reducing *LGR6* expression, with the 6-fold increase in *LGR5* expression unable to rescue this (Figure S9B). Furthermore, we utilized this bulk RNA-seq dataset to probe for the ECM signatures we noted above, and ToppFun pathway analyses identified a strong signature for ECM-related processes in the two patients analyzed (Table S4), validating our observations in the SCT-derived GSEAs that ECM-related pathways are enriched in WβA cells. This suggests that localized ECM remodeling within the physical niche of FT stem/WβA cells in organoids (and potentially *in vivo*) may play a crucial role in maintaining stem cell self-renewal and multipotency, as reported for other tissues.[58–60]

## DISCUSSION

In this study, we optimize hFT culture conditions that enable us to conduct functional analyses on stem cell renewal requirements. We also devise a strategy for biomarking, isolation, and transcriptomic characterization of putative stem cells, generating an SCT dataset of hFT organoids. Our work establishes the essentiality of WβS for FT renewal and delineates the molecular factors that regulate this renewal program (Figure 7A). Further biochemical work is required to conclusively establish the signaling mode of WNT7A in the FTs (Figure 7B). However, our identification of WNT7A's essentiality to FT maintenance is consistent with evidence from *Wnt7a* knockout mice, which contain no oviducts or severely compromised oviducts with diminished invaginations as well as global abnormalities in the correct patterning of the neonatal FRT.[61]

### WNT7A, stem cells, and the ECM

Our work provides a comprehensive characterization of WβA/FT stem cells. In particular, our GSEAs point to a dominant role played by ECM processes in maintaining WβA/FT stem cells. Indeed, WNT7A, which we identify as the factor maintaining WβA/FT stem cells, has been shown to synergize with fibronectin and SDC4[62,63] or integrin-β1 and Decorin[64] in regulating renewal of muscle satellite and neuroepithelium progenitors, respectively. In a pathological context, tumor-secreted WNT7A has been shown to remodel the underlying ECM, enable tumor invasion, and predict a poor prognosis across various cancers[65–71] by recruiting and activating TGF-β signaling in cancer-associated fibroblasts[65] or by inducing epithelial secretion of ECM remodeling enzymes such as MMP7[67] or MMP1 and MMP10.[68] Further functional studies are required to elucidate ECM-driven maintenance of FT stem cells and to establish

**Figure 6. Single Cell Transcriptomic characterization of hFT WβA cells**

(A) UMAP dimensionality reduction of the single-cell transcriptomes of WβA (GFP+) and non-WβA (GFP−) cells. Cells were FACS isolated from patient-derived hFT WβS-reporter organoids and processed using the SMART-seq2 protocol for scRNA-seq. UMAPs are shown by patient (left), WβS status (center), or clusters (right).

(B) Heatmap showing significant ($p < 0.05$) patient-shared differentially expressed genes (DEGs) derived from intra-patient comparison of the single-cell transcriptomes of WβA vs. non-WβA cells. Each column represents a single cell. Each row represents a shared DEG. Heatmap colors indicate expression level as shown in the bar.

(C) Violin plots showing the single-cell expression profile of specific DEGs that mark WβA cells (green, top) or non-WβA cells (red, bottom). Each dot represents a cell (n = 3 patients).

(D) Bubble plot showing the results of intra-patient GSEA of pathways that are consistently upregulated (green, positive normalized enrichment score [NES]) or downregulated (red, negative NES) in WβA cells relative to non-WβA cells across patients. Each row represents a pathway. Blue text indicates the gene set collection from which the pathway is derived. Purple arrows point to ECM-related pathways. Orange arrows point to gene sets associated with ovarian and mammary biology and cancer, including female hormone response. padj, adjusted p value; CHEMGENPERTURB, chemical and genetic perturbations; GOBP, Gene Ontology biological processes; GOCC, Gene Ontology cellular component.

(E) Enrichment plots for patient-shared, ECM-related pathways shown in (D). GSEA enrichment plots for patient-unique ECM-related processes can be found in Table S3.

(F) Heatmap showing hierarchical clustering of the shared DEGs from the bulk RNA-seq of WβA and non-WβA cells derived from WβS-reporter organoids established from 2 patients.

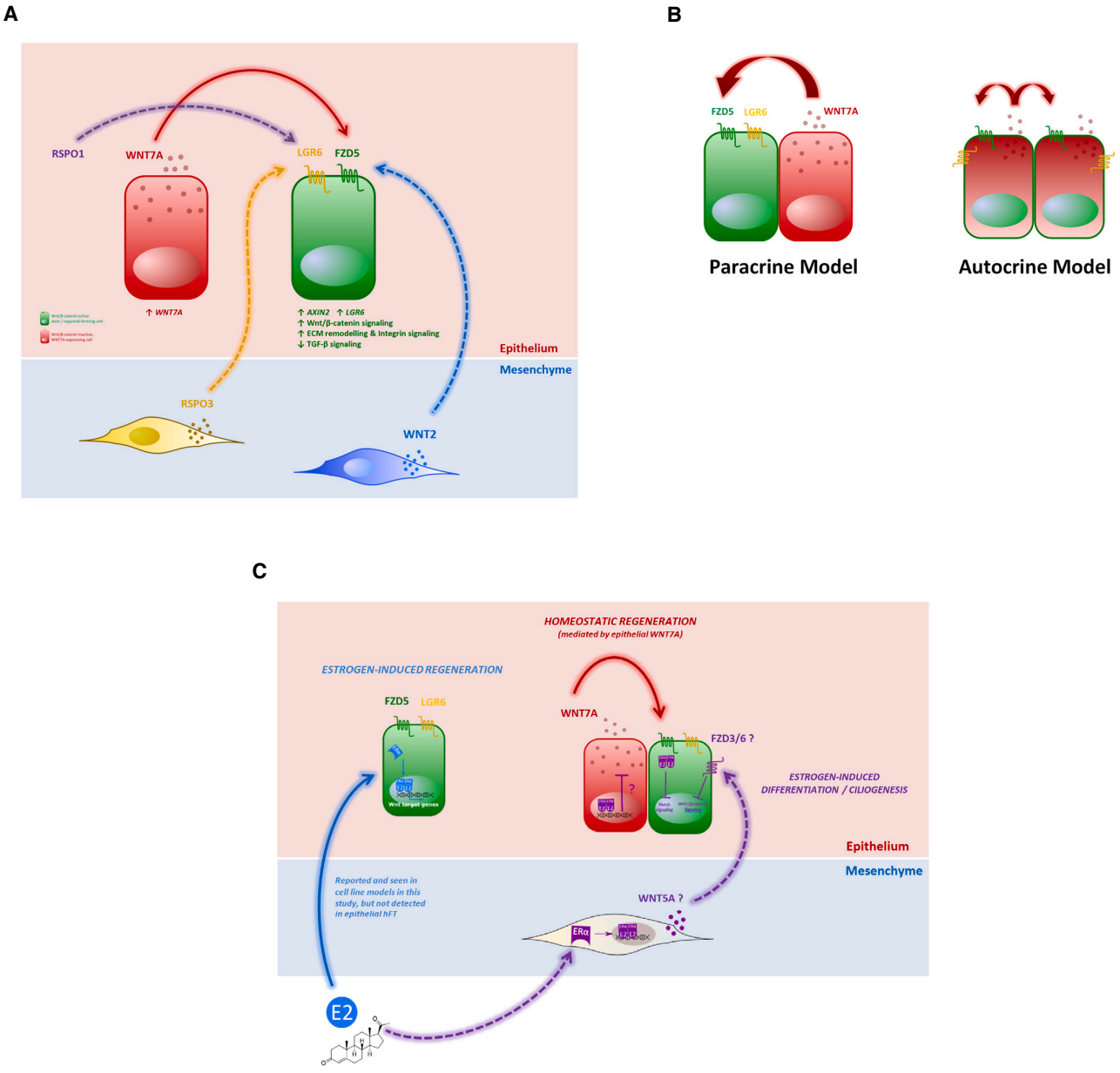


**Figure 7. Working model on the molecular maintenance of FT stem cells**

Shown are depictions of the proposed molecular maintenance (A), signaling mode (B), and hormonal regulation (C) of FT stem cells. Dashed lines represent hypothesized interactions not shown in this study. WβA cells are depicted in green; non-WβA cells are depicted in red.

the molecular mechanisms, if any, of WNT7A's remodeling of the FT ECM.

## WβA cells and mouse models

Axin2 and Lgr5 are universal WβS target genes.[25] Lineage tracing in adult mice has shown that *Lgr5*+ cells do not contribute to mOV homeostasis.[72] Although *Lgr5* specifically marks homeostatic WβA adult stem cells in various tissues, including the intestine[23,73] and the pyloric stomach,[74] *Axin2* is a better marker of homeostatic WβA stem cells in other tissue systems, such as the liver,[75,76] stomach (corpus) region,[77,78] adult vagina,[72,79] and endometrium,[80,81] which shares embryonic origins and a developmental continuum with the oviduct. Based on this and our data, we propose *Axin2*, *Lgr6*, or genes derived from our SCT panel of highly differentially expressed genes (Figure 6C) as strong candidates for marking putative FT/oviduct stem cells in future lineage tracing studies.

## hFT versus mOV regeneration

While our work underscores the essentiality of WβS for regeneration of hFT organoids, other reports have shown that regeneration of mOV organoids is WβS independent.[3,82] We extend this

observation to show that mOV organoid regeneration is unaffected by extracellular upstream or intracellular downstream inhibition of WβS. Data from our WβS-reporter organoids and RNA FISH suggest that a WNT7A-FZD5 signaling axis also regulates WβS in mOV organoids, but unlike in the human setting, this signaling axis is not essential for renewal of mOV stem cells *in vitro*. Similarly, TGF-β signaling inhibition, which is essential for hFT organoid renewal, is dispensable for mOV organoid regeneration. We find these differences to be striking and to warrant further investigation.

### Hormonal regulation of the FT stem cell niche

Our findings suggest that estrogen-ERα can circumvent the cellular WβS pathway to activate transcription of WβS target genes. However, in the presence of WNT7A (hFT organoids and WNT7A-overexpressing HEK293 cells), we find that estrogen suppresses WNT7A protein and WNT7A-induced WβS, and in hFT organoids, estrogen downregulates *WNT7A* mRNA. The estrogenic inhibitory effect we see on WNT7A is consistent with previous reports from human[83] and mouse[50,84,85] studies. Furthermore, we find that estrogen potently induces ciliogenesis by dual inhibition of WβS and Notch signaling, identifying precise *in vitro* conditions to establish long-term patient-derived ciliated cell models that can serve as useful tools for the study of ciliogenesis and ciliopathies.[86,87] Overall, we propose a working model of hormonal regulation of the putative FT stem cell niche (Figure 7C).

### Conclusions

In summary, we provide a deep characterization of FT stem cells and the molecular determinants of their renewal and cell fate specification. Our work lays the foundation for subsequent functional and *in vivo* studies on FT homeostasis, disease, hormonal regulation, and epithelial-mesenchymal cross-talk. Our findings provide a basis for mechanistic work investigating the role of FT stem cells in ovarian cancer initiation.

### Limitations of the study

We acknowledge a few limitations in our study. Firstly, our data do not show a direct link between WNT7A/LGR6 and OFE; for instance, by RNA-based knockdown or protein-based rescue of WNT-blocked organoids, for the reasons discussed. For WNT7A, it is envisioned that ongoing deep structural studies and bioengineering efforts will, in the future, make available WNT7A-monospecific mimetics that will help address this question.

Second, our work did not investigate whether the mesenchymally derived *WNT2* and *RSPO3* ligands we identified could potentially render *WNT7A* redundant to organoid regeneration *in vitro* or tissue homeostasis *in vivo*. Third, our bulk and scRNA-seq data point to a contribution of ECM processes to maintaining FT stem cells, and this awaits future functional work to confirm this. On estrogen signaling, cells are known to elicit distinct responses to estrogen based on its local concentration, and the cycling nature and physiological doses of estrogen *in vivo* are difficult to recapitulate *in vitro*. Therefore, the phenotypes observed in estrogen-supplemented organoids, while providing a preliminary understanding of estrogenic molecular changes, are likely not to capture the full spectrum of molecular and phenotypic changes induced by estrogen *in vivo*. To address this, we propose the optimization of complex hFT organoid co-culture methods incorporating epithelial and stromal compartments to dissect these estrogenic changes as well as to study the influence of mesenchymally derived factors, such as WNT2 and RSPO3, on FT stem cells.

## STAR★METHODS

Detailed methods are provided in the online version of this paper and include the following:

- KEY RESOURCES TABLE
- RESOURCE AVAILABILITY
  - Lead contact
  - Materials availability
  - Data and code availability
- EXPERIMENTAL MODEL AND STUDY PARTICIPANT DETAILS
  - Human subjects and tissue Acquisition
  - Mouse tissue Acquisition
- METHOD DETAILS
  - Tissue dissociation & primary Culture
  - Human Fallopian tube Organoid Culture
  - Mouse oviduct Organoid Culture
  - Organoid formation efficiency (OFE) assay
  - Generation of WβS-reporter organoids
  - scRNA-seq of WβS-reporter organoids
  - Bulk RNA-seq of WβS-reporter organoids
  - Organoid RNA extraction & RT-qPCR
  - RNA In situ Hybridization (RNAScope)
  - Organoid Immunofluorescence staining
  - Wnt-reporter/TOPFlash assay
  - Cell Culture, protein expression & Western blotting
- QUANTIFICATION AND STATISTICAL ANALYSIS
  - Single Cell RNA-seq analysis
  - Bulk RNA-seq analysis

## SUPPLEMENTAL INFORMATION

Supplemental information can be found online at https://doi.org/10.1016/j.celrep.2023.113354.

## ACKNOWLEDGMENTS

We are grateful to the Weatherall Institute of Molecular Medicine (WIMM) FACS core facility, the WIMM Wolfson Imaging Center, and the WIMM Single Cell Core Facility for help in this study. We thank Dr. M. Angelica Martinez-Gakidis for valuable editorial feedback. This work was supported by Ovarian Cancer Action, the Oxford Biomedical Research Centre, the National Institute for Health Research, and the Diane Oxberry Trust.

## AUTHOR CONTRIBUTIONS

Conceptualization, A.A. and A.A.A.; project administration, A.A. and A.A.A.; supervision, A.A.A.; funding acquisition, A.A.A. and J.S.B; investigation, A.A., M.A., Z.H., N.W., M.M., L.S.G., and A.A.A.; data curation, A.A., M.A., Z.H., N.W., M.M., L.S.G., J.S.B., and A.A.A; scRNA-seq and analysis, M.A., Z.H., and F.S.; bulk RNA-seq and analysis, M.A.; methodology, formal analysis, and visualization, A.A. and A.A.A.; writing – original draft, A.A. and A.A.A.; writing – review & editing, A.A., J.S.B., and A.A.A.; generation of

anti-FZD5 antibodies, S.S.S., J.A., and L.L.B.; resources (clinical samples), N.W., M.M., H.S.m., M.A., J.J., and B.A.

## DECLARATION OF INTERESTS

The authors declare no competing interests.

## INCLUSION AND DIVERSITY

We support inclusive, diverse, and equitable conduct of research.

Received: April 4, 2023
Revised: July 31, 2023
Accepted: October 11, 2023

## REFERENCES

1. Erickson, B.K., Conner, M.G., and Landen, C.N. (2013). The role of the fallopian tube in the origin of ovarian cancer. Am. J. Obstet. Gynecol. *209*, 409–414. https://doi.org/10.1016/j.ajog.2013.04.019.
2. Ghosh, A., Syed, S.M., and Tanwar, P.S. (2017). In Vivo Genetic Cell Lineage Tracing Reveals that Oviductal Secretory Cells Self-Renew and Give Rise to Ciliated Cells, 149989. https://doi.org/10.1242/dev.
3. Xie, Y., Park, E.-S., Xiang, D., and Li, Z. (2018). Long-term organoid culture reveals enrichment of organoid-forming epithelial cells in the fimbrial portion of mouse fallopian tube. Stem Cell Res. *32*, 51–60. https://doi.org/10.1016/J.SCR.2018.08.021.
4. Wang, Y., Sacchetti, A., van Dijk, M.R., van der Zee, M., van der Horst, P.H., Joosten, R., Burger, C.W., Grootegoed, J.A., Blok, L.J., and Fodde, R. (2012). Identification of Quiescent, Stem-Like Cells in the Distal Female Reproductive Tract. PLoS One *7*, e40691. https://doi.org/10.1371/JOURNAL.PONE.0040691.
5. Zhu, M., Iwano, T., and Takeda, S. (2020). Fallopian tube basal stem cells reproducing the epithelial sheets in vitro—stem cell of fallopian epithelium. Biomolecules *10*, 1270. https://doi.org/10.3390/biom10091270.
6. Snegovskikh, V., Mutlu, L., Massasa, E., and Taylor, H.S. (2014). Identification of putative fallopian tube stem cells. Reprod. Sci. *21*, 1460–1464. https://doi.org/10.1177/1933719114553448.
7. Paik, D.Y., Janzen, D.M., Schafenacker, A.M., Velasco, V.S., Shung, M.S., Cheng, D., Huang, J., Witte, O.N., and Memarzadeh, S. (2012). Stem-Like Epithelial Cells Are Concentrated in the Distal End of the Fallopian Tube: A Site for Injury and Serous Cancer Initiation. Stem Cell. *30*, 2487–2497. https://doi.org/10.1002/stem.1207.
8. Yamamoto, Y., Ning, G., Howitt, B.E., Mehra, K., Wu, L., Wang, X., Hong, Y., Kern, F., Wei, T.S., Zhang, T., et al. (2016). *In vitro* and *in vivo* correlates of physiological and neoplastic human Fallopian tube stem cells. J. Pathol. *238*, 519–530. https://doi.org/10.1002/path.4649.
9. Kessler, M., Hoffmann, K., Brinkmann, V., Thieck, O., Jackisch, S., Toelle, B., Berger, H., Mollenkopf, H.-J., Mangler, M., Sehouli, J., et al. (2015). The Notch and Wnt pathways regulate stemness and differentiation in human fallopian tube organoids. Nat. Commun. *6*, 8989. https://doi.org/10.1038/ncomms9989.
10. Hu, Z., Artibani, M., Alsaadi, A., Wietek, N., Morotti, M., Shi, T., Zhong, Z., Santana Gonzalez, L., El-Sahhar, S., Carrami, E.M., et al. (2020). The Repertoire of Serous Ovarian Cancer Non-genetic Heterogeneity Revealed by Single-Cell Sequencing of Normal Fallopian Tube Epithelial Cells. Cancer Cell *37*, 226–242.e7. https://doi.org/10.1016/j.ccell.2020.01.003.
11. Dinh, H.Q., Lin, X., Abbasi, F., Nameki, R., Haro, M., Olingy, C.E., Chang, H., Hernandez, L., Gayther, S.A., Wright, K.N., et al. (2021). Single-cell transcriptomics identifies gene expression networks driving differentiation and tumorigenesis in the human fallopian tube. Cell Rep. *35*, 108978. https://doi.org/10.1016/j.celrep.2021.108978.
12. Labidi-Galy, S.I., Papp, E., Hallberg, D., Niknafs, N., Adleff, V., Noe, M., Bhattacharya, R., Novak, M., Jones, S., Phallen, J., et al. (2017). High grade serous ovarian carcinomas originate in the fallopian tube. Nat. Commun. *8*, 1093. https://doi.org/10.1038/s41467-017-00962-1.
13. Kuhn, E., Kurman, R.J., Vang, R., Sehdev, A.S., Han, G., Soslow, R., Wang, T.-L., and Shih, I.-M. (2012). TP53 mutations in serous tubal intraepithelial carcinoma and concurrent pelvic high-grade serous carcinoma-evidence supporting the clonal relationship of the two lesions. J. Pathol. *226*, 421–426. https://doi.org/10.1002/path.3023.
14. Kim, J., Park, E.Y., Kim, O., Schilder, J.M., Coffey, D.M., Cho, C.H., and Bast, R.C. (2018). Cell origins of high-grade serous ovarian cancer. Cancers *10*, 433. https://doi.org/10.3390/cancers10110433.
15. Kroeger, P.T., and Drapkin, R. (2017). Pathogenesis and heterogeneity of ovarian cancer. Curr. Opin. Obstet. Gynecol. *29*, 26–34. https://doi.org/10.1097/GCO.0000000000000340.
16. Gaitskell, K., Green, J., Pirie, K., Barnes, I., Hermon, C., Reeves, G.K., and Beral, V.; Million Women Study Collaborators (2018). Histological subtypes of ovarian cancer associated with parity and breastfeeding in the prospective Million Women Study. Int. J. Cancer *142*, 281–289. https://doi.org/10.1002/ijc.31063.
17. Zeng, J., Alvarez-Yela, A.C., Casarez, E., Jiang, Y., Wang, L., Kelly, B.E., Jenkins, T., Ke, E., Atkins, K.A., Janes, K.A., et al. (2023). Dichotomous ovarian cancer-initiating potential of Pax8+ cells revealed by a mouse genetic mosaic model. iScience *26*, 106742. https://doi.org/10.1016/J.ISCI.2023.106742.
18. Tojo, M., Hamashima, Y., Hanyu, A., Kajimoto, T., Saitoh, M., Miyazono, K., Node, M., and Imamura, T. (2005). The ALK-5 inhibitor A-83-01 inhibits Smad signaling and epithelial-to-mesenchymal transition by transforming growth factor-beta. Cancer Sci. *96*, 791–800. https://doi.org/10.1111/j.1349-7006.2005.00103.x.
19. Hao, H.X., Xie, Y., Zhang, Y., Charlat, O., Oster, E., Avello, M., Lei, H., Mickanin, C., Liu, D., Ruffner, H., et al. (2012). ZNRF3 promotes Wnt receptor turnover in an R-spondin-sensitive manner. Nature *485*, 195–200. https://doi.org/10.1038/nature11019.
20. Koo, B.K., Spit, M., Jordens, I., Low, T.Y., Stange, D.E., Van De Wetering, M., Van Es, J.H., Mohammed, S., Heck, A.J.R., Maurice, M.M., and Clevers, H. (2012). Tumour suppressor RNF43 is a stem-cell E3 ligase that induces endocytosis of Wnt receptors. Nature *488*, 665–669. https://doi.org/10.1038/nature11308.
21. Huang, S.M.A., Mishina, Y.M., Liu, S., Cheung, A., Stegmeier, F., Michaud, G.A., Charlat, O., Wiellette, E., Zhang, Y., Wiessner, S., et al. (2009). Tankyrase inhibition stabilizes axin and antagonizes Wnt signalling. Nature *461*, 614–620. https://doi.org/10.1038/nature08356.
22. Okazaki, H., Sato, S., Koyama, K., Morizumi, S., Abe, S., Azuma, M., Chen, Y., Goto, H., Aono, Y., Ogawa, H., et al. (2019). The novel inhibitor PRI-724 for Wnt/β-catenin/CBP signaling ameliorates bleomycin-induced pulmonary fibrosis in mice. Exp. Lung Res. *45*, 188–199. https://doi.org/10.1080/01902148.2019.1638466.
23. Sato, T., van Es, J.H., Snippert, H.J., Stange, D.E., Vries, R.G., van den Born, M., Barker, N., Shroyer, N.F., van de Wetering, M., and Clevers, H. (2011). Paneth cells constitute the niche for Lgr5 stem cells in intestinal crypts. Nature *469*, 415–418. https://doi.org/10.1038/nature09637.
24. Fuerer, C., and Nusse, R. (2010). Lentiviral vectors to probe and manipulate the Wnt signaling pathway. PLoS One *5*, e9370. https://doi.org/10.1371/journal.pone.0009370.
25. Boonekamp, K.E., Heo, I., Artegiani, B., Asra, P., van Son, G., de Ligt, J., and Clevers, H. (2021). Identification of novel human Wnt target genes using adult endodermal tissue-derived organoids. Dev. Biol. *474*, 37–47. https://doi.org/10.1016/j.ydbio.2021.01.009.
26. Picelli, S., Faridani, O.R., Björklund, A.K., Winberg, G., Sagasser, S., and Sandberg, R. (2014). Full-length RNA-seq from single cells using Smart-seq2. Nat. Protoc. *9*, 171–181. https://doi.org/10.1038/nprot.2014.006.

27. Park, S., Cui, J., Yu, W., Wu, L., Carmon, K.S., and Liu, Q.J. (2018). Differential activities and mechanisms of the four r-spondins in potentiating wnt/-catenin signaling. J. Biol. Chem. *293*, 9759–9769. https://doi.org/10.1074/JBC.RA118.002743/ATTACHMENT/7D21F42A-0024-4AE9-A571-DB0E05669870/MMC1.PDF.

28. Tüysüz, N., van Bloois, L., van den Brink, S., Begthel, H., Verstegen, M.M.A., Cruz, L.J., Hui, L., van der Laan, L.J.W., de Jonge, J., Vries, R., et al. (2017). Lipid-mediated Wnt protein stabilization enables serum-free culture of human organ stem cells. Nat. Commun. *8*, 14578. https://doi.org/10.1038/ncomms14578.

29. Farin, H.F., Jordens, I., Mosa, M.H., Basak, O., Korving, J., Tauriello, D.V.F., de Punder, K., Angers, S., Peters, P.J., Maurice, M.M., and Clevers, H. (2016). Visualization of a short-range Wnt gradient in the intestinal stem-cell niche. Nature *530*, 340–343. https://doi.org/10.1038/nature16937.

30. Goldstein, B., Takeshita, H., Mizumoto, K., and Sawa, H. (2006). Wnt signals can function as positional cues in establishing cell polarity. Dev. Cell *10*, 391–396. https://doi.org/10.1016/j.devcel.2005.12.016.

31. Alexandre, C., Baena-Lopez, A., and Vincent, J.-P. (2013). Patterning and growth control by membrane-tethered Wingless. Nature *505*, 180–185. https://doi.org/10.1038/nature12879.

32. Dong, B., Vold, S., Olvera-Jaramillo, C., and Chang, H. (2018). Functional redundancy of frizzled 3 and frizzled 6 in planar cell polarity control of mouse hair follicles. Development *145*. https://doi.org/10.1242/dev.168468.

33. Yu, H., Ye, X., Guo, N., and Nathans, J. (2012). Frizzled 2 and frizzled 7 function redundantly in convergent extension and closure of the ventricular septum and palate: evidence for a network of interacting genes. Development *139*, 4383–4394. https://doi.org/10.1242/dev.083352.

34. Voloshanenko, O., Gmach, P., Winter, J., Kranz, D., and Boutros, M. (2017). Mapping of Wnt-Frizzled interactions by multiplex CRISPR targeting of receptor gene families. Faseb. J. *31*, 4832–4844. https://doi.org/10.1096/fj.201700144R.

35. Caricasole, A., Ferraro, T., Iacovelli, L., Barletta, E., Caruso, A., Melchiorri, D., Terstappen, G.C., and Nicoletti, F. (2003). Functional Characterization of WNT7A Signaling in PC12 Cells: INTERACTION WITH A FZD5·LRP6 RECEPTOR COMPLEX AND MODULATION BY DICKKOPF PROTEINS. J. Biol. Chem. *278*, 37024–37031. https://doi.org/10.1074/JBC.M300191200.

36. Carmon, K.S., and Loose, D.S. (2008). Wnt7a interaction with Fzd5 and detection of signaling activation using a split eGFP. Biochem. Biophys. Res. Commun. *368*, 285–291. https://doi.org/10.1016/j.bbrc.2008.01.088.

37. Steinhart, Z., Pavlovic, Z., Chandrashekhar, M., Hart, T., Wang, X., Zhang, X., Robitaille, M., Brown, K.R., Jaksani, S., Overmeer, R., et al. (2017). Genome-wide CRISPR screens reveal a Wnt–FZD5 signaling circuit as a druggable vulnerability of RNF43-mutant pancreatic tumors. Nat. Med. *23*, 60–68. https://doi.org/10.1038/nm.4219.

38. Janda, C.Y., Dang, L.T., You, C., Chang, J., de Lau, W., Zhong, Z.A., Yan, K.S., Marecic, O., Siepe, D., Li, X., et al. (2017). Surrogate Wnt agonists that phenocopy canonical Wnt and β-catenin signalling. Nature *545*, 234–237. https://doi.org/10.1038/nature22306.

39. Carmon, K.S., Gong, X., Lin, Q., Thomas, A., and Liu, Q. (2011). R-spondins function as ligands of the orphan receptors LGR4 and LGR5 to regulate Wnt/β-catenin signaling *108*, 11452–11457. https://doi.org/10.1073/pnas.1106083108.

40. Glinka, A., Dolde, C., Kirsch, N., Huang, Y.L., Kazanskaya, O., Ingelfinger, D., Boutros, M., Cruciat, C.M., and Niehrs, C. (2011). LGR4 and LGR5 are R-spondin receptors mediating Wnt/β-catenin and Wnt/PCP signalling. EMBO Rep. *12*, 1055–1061. https://doi.org/10.1038/embor.2011.175.

41. de Lau, W., Barker, N., Low, T.Y., Koo, B.-K., Li, V.S.W., Teunissen, H., Kujala, P., Haegebarth, A., Peters, P.J., van de Wetering, M., et al. (2011). Lgr5 homologues associate with Wnt receptors and mediate R-spondin signalling. Nature *476*, 293–297. https://doi.org/10.1038/nature10337.

42. Fujii, M., Shimokawa, M., Date, S., Takano, A., Matano, M., Nanki, K., Ohta, Y., Toshimitsu, K., Nakazato, Y., Kawasaki, K., et al. (2016). A Colorectal Tumor Organoid Library Demonstrates Progressive Loss of Niche Factor Requirements during Tumorigenesis. Cell Stem Cell *18*, 827–838. https://doi.org/10.1016/J.STEM.2016.04.003.

43. Seino, T., Kawasaki, S., Shimokawa, M., Tamagawa, H., Toshimitsu, K., Fujii, M., Ohta, Y., Matano, M., Nanki, K., Kawasaki, K., et al. (2018). Human Pancreatic Tumor Organoids Reveal Loss of Stem Cell Niche Factor Dependence during Disease Progression. Cell Stem Cell *22*, 454–467.e6. https://doi.org/10.1016/j.stem.2017.12.009.

44. Drost, J., van Jaarsveld, R.H., Ponsioen, B., Zimberlin, C., van Boxtel, R., Buijs, A., Sachs, N., Overmeer, R.M., Offerhaus, G.J., Begthel, H., et al. (2015). Sequential cancer mutations in cultured human intestinal stem cells. Nature *521*, 43–47. https://doi.org/10.1038/nature14415.

45. Matano, M., Date, S., Shimokawa, M., Takano, A., Fujii, M., Ohta, Y., Watanabe, T., Kanai, T., and Sato, T. (2015). Modeling colorectal cancer using CRISPR-Cas9–mediated engineering of human intestinal organoids. Nat. Med. *21*, 256–262. https://doi.org/10.1038/nm.3802.

46. Hideyuki, N., Saito, T., Yamasaki, H., Mizumoto, H., Ito, E., and Kudo, R. (1999). Nuclear localization of β-catenin in normal and carcinogenic endometrium. Mol. Carcinog. *25*, 207–218. https://doi.org/10.1002/(SICI)1098-2744(199907)25:3<207::AID-MC7>3.0.CO;2-4.

47. Kouzmenko, A.P., Takeyama, K.I., Ito, S., Furutani, T., Sawatsubashi, S., Maki, A., Suzuki, E., Kawasaki, Y., Akiyama, T., Tabata, T., and Kato, S. (2004). Wnt/β-catenin and estrogen signaling converge in vivo. J. Biol. Chem. *279*, 40255–40258. https://doi.org/10.1074/jbc.C400331200.

48. Hou, Y.F., Yuan, S.T., Li, H.C., Wu, J., Lu, J.S., Liu, G., Lu, L.J., Shen, Z.Z., Ding, J., and Shao, Z.M. (2004). ERβ exerts multiple stimulative effects on human breast carcinoma cells. Oncogene *23*, 5799–5806. https://doi.org/10.1038/sj.onc.1207765.

49. McLachlan, J.A., Newbold, R.R., and Bullock, B.C. (1980). Long-Term Effects on the Female Mouse Genital Tract Associated with Prenatal Exposure to Diethylstilbestrol. Cancer Res. *40*, 3988–3999.

50. Couse, J.F., Dixon, D., Yates, M., Moore, A.B., Ma, L., Maas, R., and Korach, K.S. (2001). Estrogen receptor-α knockout mice exhibit resistance to the developmental effects of neonatal diethylstilbestrol exposure on the female reproductive tract. Dev. Biol. *238*, 224–238. https://doi.org/10.1006/dbio.2001.0413.

51. Wagner, J., and Lehmann, L. (2006). Estrogens modulate the gene expression of Wnt-7a in cultured endometrial adenocarcinoma cells. In Molecular Nutrition and Food Research, pp. 368–372. https://doi.org/10.1002/mnfr.200500215.

52. Yin, X., Farin, H.F., van Es, J.H., Clevers, H., Langer, R., and Karp, J.M. (2014). Niche-independent high-purity cultures of Lgr5+ intestinal stem cells and their progeny. Nat. Methods *11*, 106–112. https://doi.org/10.1038/nmeth.2737.

53. Broutier, L., Andersson-Rolf, A., Hindley, C.J., Boj, S.F., Clevers, H., Koo, B.-K., and Huch, M. (2016). Culture and establishment of self-renewing human and mouse adult liver and pancreas 3D organoids and their genetic manipulation. Nat. Protoc. *11*, 1724–1743. https://doi.org/10.1038/nprot.2016.097.

54. Loomans, C.J.M., Williams Giuliani, N., Balak, J., Ringnalda, F., van Gurp, L., Huch, M., Boj, S.F., Sato, T., Kester, L., de Sousa Lopes, S.M.C., et al. (2018). Expansion of Adult Human Pancreatic Tissue Yields Organoids Harboring Progenitor Cells with Endocrine Differentiation Potential. Stem Cell Rep. *10*, 712–724. https://doi.org/10.1016/J.STEMCR.2018.02.005.

55. You, Y., Huang, T., Richer, E.J., Schmidt, J.E.H., Zabner, J., Borok, Z., and Brody, S.L. (2004). Role of f-box factor foxj1 in differentiation of ciliated airway epithelial cells. Am. J. Physiol. Lung Cell Mol. Physiol. *286*, L650–L657. https://doi.org/10.1152/ajplung.00170.2003.

56. Kaur, A., Lim, J.Y.S., Sepramaniam, S., Patnaik, S., Harmston, N., Lee, M.A., Petretto, E., Virshup, D.M., and Madan, B. (2021). WNT inhibition creates a BRCA-like state in Wnt-addicted cancer. EMBO Mol. Med. *13*, e13349. https://doi.org/10.15252/EMMM.202013349.

57. Angers, S. (2021). Wnt signaling inhibition confers induced synthetic lethality to PARP inhibitors. EMBO Mol. Med. *13*, e14002. https://doi.org/10.15252/EMMM.202114002.

58. Guilak, F., Cohen, D.M., Estes, B.T., Gimble, J.M., Liedtke, W., and Chen, C.S. (2009). Control of Stem Cell Fate by Physical Interactions with the Extracellular Matrix. Cell Stem Cell *5*, 17–26. https://doi.org/10.1016/J.STEM.2009.06.016.

59. Gattazzo, F., Urciuolo, A., and Bonaldo, P. (2014). Extracellular matrix: A dynamic microenvironment for stem cell niche. Biochim. Biophys. Acta *1840*, 2506–2519. https://doi.org/10.1016/J.BBAGEN.2014.01.010.

60. Watt, F.M., and Huck, W.T.S. (2013). Role of the extracellular matrix in regulating stem cell fate. Nat. Rev. Mol. Cell Biol. *14*, 467–473. https://doi.org/10.1038/nrm3620.

61. Miller, C., and Sassoon, D.A. (1998). Wnt-7a maintains appropriate uterine patterning during the development of the mouse female reproductive tract. Development *125*. https://doi.org/10.1242/dev.125.16.3201.

62. Moyle, L.A., Cheng, R.Y., Liu, H., Davoudi, S., Ferreira, S.A., Nissar, A.A., Sund, Y., Gentleman, E., Simmons, C.A., and Gilbert, P.M. (2020). Three-dimensional niche stiffness synergizes with Wnt7a to modulate the extent of satellite cell symmetric self-renewal divisions. Mol. Biol. Cell *31*, 1703–1713, /ASSET/IMAGES/LARGE/MBC-31-1703-G004.JPEG. https://doi.org/10.1091/MBC.E20-01-0078.

63. Bentzinger, C.F., Wang, Y.X., Von Maltzahn, J., Soleimani, V.D., Yin, H., and Rudnicki, M.A. (2013). Fibronectin Regulates Wnt7a Signaling and Satellite Cell Expansion. Cell Stem Cell *12*, 75–87. https://doi.org/10.1016/J.STEM.2012.09.015.

64. Long, K., Moss, L., Laursen, L., Boulter, L., and Ffrench-Constant, C. (2016). Integrin signalling regulates the expansion of neuroepithelial progenitors and neurogenesis via Wnt7a and Decorin. Nat. Commun. *7*, 10354. https://doi.org/10.1038/ncomms10354.

65. Avgustinova, A., Iravani, M., Robertson, D., Fearns, A., Gao, Q., Klingbeil, P., Hanby, A.M., Speirs, V., Sahai, E., Calvo, F., and Isacke, C.M. (2016). Tumour cell-derived Wnt7a recruits and activates fibroblasts to promote tumour aggressiveness. Nat. Commun. *7*, 10305–10314. https://doi.org/10.1038/ncomms10305.

66. Liu, Y., Meng, F., Xu, Y., Yang, S., Xiao, M., Chen, X., and Lou, G. (2013). Overexpression of wnt7a is associated with tumor progression and unfavorable prognosis in endometrial cancer. Int. J. Gynecol. Cancer *23*, 304–311. https://doi.org/10.1097/IGC.0b013e31827c7708.

67. Yoshioka, S., King, M.L., Ran, S., Okuda, H., MacLean, J.A., McAsey, M.E., Sugino, N., Brard, L., Watabe, K., and Hayashi, K. (2012). WNT7A Regulates Tumor Growth and Progression in Ovarian Cancer through the WNT/-Catenin Pathway. Mol. Cancer Res. *10*, 469–482. https://doi.org/10.1158/1541-7786.MCR-11-0177.

68. Huang, X., Zhu, H., Gao, Z., Li, J., Zhuang, J., Dong, Y., Shen, B., Li, M., Zhou, H., Guo, H., et al. (2018). Wnt7a activates canonical Wnt signaling, promotes bladder cancer cell invasion, and is suppressed by MIR-370-3p. J. Biol. Chem. *293*, 6693–6706. https://doi.org/10.1074/jbc.RA118.001689.

69. King, M.L., Lindberg, M.E., Stodden, G.R., Okuda, H., Ebers, S.D., Johnson, A., Montag, A., Lengyel, E., MacLean Ii, J.A., and Hayashi, K. (2015). WNT7A/β-catenin signaling induces FGF1 and influences sensitivity to niclosamide in ovarian cancer. Oncogene *34*, 3452–3462. https://doi.org/10.1038/onc.2014.277.

70. Zhang, X.L., Peng, C.J., Peng, J., Jiang, L.Y., Ning, X.M., and Zheng, J.H. (2010). Prognostic role of Wnt7a expression in ovarian carcinoma patients. Neoplasma *57*, 545–551.

71. Jia, B., Qiu, X., Chu, H., Sun, X., Xu, S., Zhao, X., and Zhao, J. (2019). Wnt7a predicts poor prognosis, and contributes to growth and metastasis in tongue squamous cell carcinoma. Oncol. Rep. *41*, 1749–1758. https://doi.org/10.3892/OR.2019.6974/HTML.

72. Ng, A., Tan, S., Singh, G., Rizk, P., Swathi, Y., Tan, T.Z., Huang, R.Y.J., Leushacke, M., and Barker, N. (2014). Lgr5 marks stem/progenitor cells in ovary and tubal epithelia. Nat. Cell Biol. *16*, 745–757. https://doi.org/10.1038/ncb3000.

73. Barker, N., Van Es, J.H., Kuipers, J., Kujala, P., Van Den Born, M., Cozijnsen, M., Haegebarth, A., Korving, J., Begthel, H., Peters, P.J., and Clevers, H. (2007). Identification of stem cells in small intestine and colon by marker gene Lgr5. Nature *449*, 1003–1007. https://doi.org/10.1038/nature06196.

74. Barker, N., Huch, M., Kujala, P., van de Wetering, M., Snippert, H.J., van Es, J.H., Sato, T., Stange, D.E., Begthel, H., van den Born, M., et al. (2010). Lgr5+ve Stem Cells Drive Self-Renewal in the Stomach and Build Long-Lived Gastric Units In Vitro. Cell Stem Cell *6*, 25–36. https://doi.org/10.1016/j.stem.2009.11.013.

75. Wang, B., Zhao, L., Fish, M., Logan, C.Y., and Nusse, R. (2015). Self-renewing diploid Axin2 + cells fuel homeostatic renewal of the liver. Nature *524*, 180–185. https://doi.org/10.1038/nature14863.

76. Huch, M., Dorrell, C., Boj, S.F., Van Es, J.H., Li, V.S.W., Van De Wetering, M., Sato, T., Hamer, K., Sasaki, N., Finegold, M.J., et al. (2013). In vitro expansion of single Lgr5 + liver stem cells induced by Wnt-driven regeneration. Nature *494*, 247–250. https://doi.org/10.1038/nature11826.

77. Stange, D.E., Koo, B.K., Huch, M., Sibbel, G., Basak, O., Lyubimova, A., Kujala, P., Bartfeld, S., Koster, J., Geahlen, J.H., et al. (2013). Differentiated Troy+ chief cells act as reserve stem cells to generate all lineages of the stomach epithelium. Cell *155*, 357–368. https://doi.org/10.1016/j.cell.2013.09.008.

78. Leushacke, M., Tan, S.H., Wong, A., Swathi, Y., Hajamohideen, A., Tan, L.T., Goh, J., Wong, E., Denil, S.L.I.J., Murakami, K., and Barker, N. (2017). Lgr5-expressing chief cells drive epithelial regeneration and cancer in the oxyntic stomach. Nat. Cell Biol. *19*, 774–786. https://doi.org/10.1038/ncb3541.

79. Ali, A., Syed, S.M., Jamaluddin, M.F.B., Colino-Sanguino, Y., Gallego-Ortega, D., and Tanwar, P.S. (2020). Cell Lineage Tracing Identifies Hormone-Regulated and Wnt-Responsive Vaginal Epithelial Stem Cells. Cell Rep. *30*, 1463–1477.e7. https://doi.org/10.1016/j.celrep.2020.01.003.

80. Seishima, R., Leung, C., Yada, S., Murad, K.B.A., Tan, L.T., Hajamohideen, A., Tan, S.H., Itoh, H., Murakami, K., Ishida, Y., et al. (2019). Neonatal Wnt-dependent Lgr5 positive stem cells are essential for uterine gland development. Nat. Commun. *10*, 5378. https://doi.org/10.1038/s41467-019-13363-3.

81. Syed, S.M., Kumar, M., Ghosh, A., Tomasetig, F., Ali, A., Whan, R.M., Alterman, D., and Tanwar, P.S. (2020). Endometrial Axin2+ Cells Drive Epithelial Homeostasis, Regeneration, and Cancer following Oncogenic Transformation. Cell Stem Cell *26*, 64–80.e13. https://doi.org/10.1016/j.stem.2019.11.012.

82. Lõhmussaar, K., Kopper, O., Korving, J., Begthel, H., Vreuls, C.P.H., van Es, J.H., and Clevers, H. (2020). Assessing the origin of high-grade serous ovarian cancer using CRISPR-modification of mouse organoids. Nat. Commun. *11*, 2660. https://doi.org/10.1038/s41467-020-16432-0.

83. Bui, T.D., Zhang, L., Rees, M.C., Bicknell, R., and Harris, A.L. (1997). Expression and hormone regulation of Wnt2, 3, 4, 5a, 7a, 7b and 10b in normal human endometrium and endometrial carcinoma. Br. J. Cancer *75*, 1131–1136. https://doi.org/10.1038/bjc.1997.195.

84. Miller, C., Pavlova, A., and Sassoon, D.A. (1998). Differential expression patterns of Wnt genes in the murine female reproductive tract during development and the estrous cycle. Mech. Dev. *76*, 91–99. https://doi.org/10.1016/S0925-4773(98)00112-9.

85. Miller, C., Degenhardt, K., and Sassoon, D.A. (1998). Fetal exposure to DES results in de-regulation of Wnt7a during uterine morphogenesis [2]. Nat. Genet. *20*, 228–230. https://doi.org/10.1038/3027.

86. Lyons, R.A., Saridogan, E., and Djahanbakhch, O. (2006). The reproductive significance of human Fallopian tube cilia. Hum. Reprod. Update *12*, 363–372. https://doi.org/10.1093/HUMUPD/DML012.

87. Raidt, J., Werner, C., Menchen, T., Dougherty, G.W., Olbrich, H., Loges, N.T., Schmitz, R., Pennekamp, P., and Omran, H. (2015). Ciliary function and motor protein composition of human fallopian tubes. Hum. Reprod. *30*, 2871–2880. https://doi.org/10.1093/HUMREP/DEV227.

88. Veeman, M.T., Slusarski, D.C., Kaykas, A., Louie, S.H., and Moon, R.T. (2003). Zebrafish prickle, a modulator of noncanonical Wnt/Fz signaling, regulates gastrulation movements. Curr. Biol. *13*, 680–685. https://doi.org/10.1016/S0960-9822(03)00240-9.

89. Najdi, R., Proffitt, K., Sprowl, S., Kaur, S., Yu, J., Covey, T.M., Virshup, D.M., and Waterman, M.L. (2012). A uniform human Wnt expression library reveals a shared secretory pathway and unique signaling activities. Differentiation. *84*, 203–213. https://doi.org/10.1016/J.DIFF.2012.06.004.

90. MacDonald, B.T., Hien, A., Zhang, X., Iranloye, O., Virshup, D.M., Waterman, M.L., and He, X. (2014). Disulfide bond requirements for active Wnt ligands. J. Biol. Chem. *289*, 18122–18136. https://doi.org/10.1074/jbc.M114.575027.

91. Mao, C., Patterson, N.M., Cherian, M.T., Aninye, I.O., Zhang, C., Montoya, J.B., Cheng, J., Putt, K.S., Hergenrother, P.J., Wilson, E.M., et al. (2008). A new small molecule inhibitor of estrogen receptor $\alpha$ binding to estrogen response elements blocks estrogen-dependent growth of cancer cells. J. Biol. Chem. *283*, 12819–12830. https://doi.org/10.1074/jbc.M709936200.

92. Su, S., Blackwelder, A.J., Grossman, G., Minges, J.T., Yuan, L., Young, S.L., and Wilson, E.M. (2012). Primate-specific Melanoma Antigen-A11 Regulates Isoform-specific Human Progesterone Receptor-B Transactivation. J. Biol. Chem. *287*, 34809–34824. https://doi.org/10.1074/JBC.M112.372797.

93. Hao, Y., Hao, S., Andersen-Nissen, E., Mauck, W.M., Zheng, S., Butler, A., Lee, M.J., Wilk, A.J., Darby, C., Zager, M., et al. (2021). Integrated analysis of multimodal single-cell data. Cell *184*, 3573–3587. https://doi.org/10.1016/J.CELL.2021.04.048/ATTACHMENT/1E5EB5C1-59EE-4B2B-8BFA-14B48A54FF8F/MMC3.

94. Robinson, M.D., McCarthy, D.J., and Smyth, G.K. (2010). edgeR: a Bioconductor package for differential expression analysis of digital gene expression data. Bioinformatics *26*, 139–140. https://doi.org/10.1093/BIOINFORMATICS/BTP616.

95. Subramanian, A., Tamayo, P., Mootha, V.K., Mukherjee, S., Ebert, B.L., Gillette, M.A., Paulovich, A., Pomeroy, S.L., Golub, T.R., Lander, E.S., and Mesirov, J.P. (2005). Gene set enrichment analysis: A knowledge-based approach for interpreting genome-wide expression profiles *102*, 15545–15550. https://doi.org/10.1073/PNAS.0506580102.

96. Sergushichev, A.A. (2016). An Algorithm for Fast Preranked Gene Set Enrichment Analysis Using Cumulative Statistic Calculation. Preprint at bioRxiv060012. https://doi.org/10.1101/060012.

97. Dobin, A., Davis, C.A., Schlesinger, F., Drenkow, J., Zaleski, C., Jha, S., Batut, P., Chaisson, M., and Gingeras, T.R. (2013). STAR: ultrafast universal RNA-seq aligner. Bioinformatics *29*, 15–21. https://doi.org/10.1093/BIOINFORMATICS/BTS635.

98. Liao, Y., Smyth, G.K., and Shi, W. (2014). featureCounts: an efficient general purpose program for assigning sequence reads to genomic features. Bioinformatics *30*, 923–930. https://doi.org/10.1093/BIOINFORMATICS/BTT656.

99. Chen, J., Bardes, E.E., Aronow, B.J., and Jegga, A.G. (2009). ToppGene Suite for gene list enrichment analysis and candidate gene prioritization. Nucleic Acids Res. *37*, W305–W311. https://doi.org/10.1093/NAR/GKP427.

100. Mora-Castilla, S., To, C., Vaezeslami, S., Morey, R., Srinivasan, S., Chousal, J.N., Cook-Andersen, H., Jenkins, J., and Laurent, L.C. (2016). Miniaturization Technologies for Efficient Single-Cell Library Preparation for Next-Generation Sequencing. J. Lab. Autom. *21*, 557–567. https://doi.org/10.1177/2211068216630741.

101. Wang, F., Flanagan, J., Su, N., Wang, L.-C., Bui, S., Nielson, A., Wu, X., Vo, H.-T., Ma, X.-J., and Luo, Y. (2012). RNAscope: A Novel in Situ RNA Analysis Platform for Formalin-Fixed, Paraffin-Embedded Tissues. J. Mol. Diagn. *14*, 22–29. https://doi.org/10.1016/j.jmoldx.2011.08.002.

102. Liberzon, A., Birger, C., Thorvaldsdóttir, H., Ghandi, M., Mesirov, J.P., and Tamayo, P. (2015). The Molecular Signatures Database Hallmark Gene Set Collection. Cell Syst. *1*, 417–425. https://doi.org/10.1016/j.cels.2015.12.004.

## STAR★METHODS

### KEY RESOURCES TABLE

| REAGENT or RESOURCE | SOURCE | IDENTIFIER |
|---|---|---|
| **Antibodies** | | |
| E-cadherin | BD Biosciences | Cat# 610181; RRID: AB_397580 |
| Ki-67 | Cell Signaling | Cat# 9027; RRID: AB_2636984 |
| PAX8 | Proteintech | Cat# 10336-1-AP; RRID: AB_2236705 |
| TUBB4 | Sigma-Aldrich | Cat# T7941; RRID: AB_261775 |
| Pan Cytokeratin | Abcam | Cat# ab7753; RRID: AB_306047 |
| c-MYC | Cell Signaling | Cat# 9402; RRID: AB_2151827 |
| WNT7A | Abcam | Cat# ab100792; RRID: AB_10858110 |
| Active β-catenin | Merck Millipore | Cat# 05–665; RRID: AB_309887 |
| V5 tag | Abcam | Cat# ab27671; RRID: AB_471093 |
| GAPDH | Proteintech | Cat# 60004-1-Ig; RRID: AB_2107436 |
| IRDye® 800CW Goat anti-Rabbit IgG Secondary Antibody | LI-COR Biosciences | Cat# 926–32211; RRID: AB_621843 |
| IRDye® 680RD Goat anti-Mouse IgG Secondary Antibody | LI-COR Biosciences | Cat# 926–68070; RRID: AB_10956588 |
| FcR blocking Reagent, human | Miltenyi Biotech | Cat# 130-059-901; RRID: AB_2892112 |
| FcR blocking Reagent, mouse | Miltenyi Biotech | Cat# 130-092-575; RRID: AB_2892833 |
| CD45-FITC, human | Biolegend | Cat# 304006; RRID: AB_314394 |
| CD45-FITC, mouse | Miltenyi Biotech | Cat# 130-116-500; RRID: AB_2727575 |
| EpCAM-APC, human | Miltenyi Biotech | Cat# 130-091-254; RRID: AB_871664 |
| EpCAM-APC, mouse | Miltenyi Biotech | Cat# 130-102-234; RRID: AB_2657519 |
| **Biological samples** | | |
| Human Fallopian tube tissue samples | Department of Gynecological Oncology, Churchill Hospital, Oxford University Hospitals | N/A |
| Mouse oviduct tissue samples | Department of Biomedical Sciences, University of Oxford | N/A |
| **Chemicals, peptides, and recombinant proteins** | | |
| Trypsin from Bovine pancreas | Sigma-Aldrich | Cat# T9935 |
| Dnase I grade II | Sigma-Aldrich | Cat# 000000010104159001 |
| Collagenase, Type I | ThermoFisher | Cat# 17018029 |
| Advanced DMEM/F-12, no phenol red | ThermoFisher | Cat# 21041033 |
| HEPES | ThermoFisher | Cat# 15630056 |
| Penicillin Streptomycin (Pen Strep) | ThermoFisher | Cat# 15070063 |
| Fetal Bovine Serum, qualified, heat inactivated, E | ThermoFisher | Cat# 10500064 |
| Epidermal Growth Factor (EGF), human, recombinant | ThermoFisher | Cat# PHG0311 |
| Noggin, human, recombinant | Peprotech | Cat# 120-10C |
| Fibroblast Growth Factor 10 (FGF-10), human, recombinant | Peprotech | Cat# 100-26 |
| Human RSPO1 | Peprotech | Cat# 120-38-100 |
| Purified mouse Rspo1 | Expressed in-house | |
| N-2 Supplement | ThermoFisher | Cat# 17502048 |
| B-27 Supplement | ThermoFisher | Cat# 12587010 |
| Nicotinamide | Sigma-Aldrich | Cat# N0636-100G |

(*Continued on next page*)

*Continued*

| REAGENT or RESOURCE | SOURCE | IDENTIFIER |
|---|---|---|
| N-Acetyl L-Cysteine | Sigma-Aldrich | Cat# A9165-5G |
| Forskolin (FSK) | Bio-Techne | Cat# 1099/10 |
| A83.01 | StemCell Technologies | Cat# 72022 |
| Y-27632 (ROCK inhibitor) | Bio-Techne | Cat# 1254/10 |
| Cultrex Organoid Harvesting Solution | Bio-Techne | Cat# 3700-100-01 |
| Matrigel (phenol red-free) | Corning | Cat# 356237 |
| Rnase A | Qiagen | Cat# 19101 |
| CHIR99021 | Bio-Techne | Cat# 4423/10 |
| IWP-2 | Bio-Techne | Cat# 3533/10 |
| LGK-974 | Stratech Scientific | Cat# S7143-SEL |
| XAV-939 | Stratech Scientific | Cat# S1180-SEL-10 mg |
| PRI-724 | Abcam | Cat# ab229168-5mg |
| Surrogate Wnt | ImmunoPrecise | Cat# N001 |
| IgG 2919 (FZD5 inhibitor) | In-house expressed (Sidhu Lab) | N/A |
| IgG 2921 (FZD5 inhibitor) | In-house expressed (Sidhu Lab) | N/A |
| Valproic Acid (VPA) | Bio-Techne | Cat# 2815/100 |
| DAPT | Bio-Techne | Cat# 2634/10 |
| Estrogen | Bio-Techne | Cat# 2824/100 |
| Progesterone | Bio-Techne | Cat# 2835/100 |
| Brefeldin A (BFA) | ThermoFisher | Cat# 00-4506-51 |
| Monensin | ThermoFisher | Cat# 00-4505-51 |
| Lenti-X Concentrator | TaKaRa Bio | Cat# 631231 |
| Polybrene Infection Reagent | Sigma-Aldrich | Cat# TR-1003-G |
| RNasin Plus RNase inhibitor | Promega | Cat# N2611 |
| dNTP Mix (10 mM ea) | ThermoFisher | Cat# 18427013 |
| Normal Donkey Serum | Sigma-Aldrich | Cat# D9663-10ML |
| VECTASHIELD anti-fade mounting medium | Vector Laboratories | Cat# H-1000 |
| **Critical commercial assays** | | |
| Dual-Luciferase Reporter Assay System | Promega | Cat# E1910 |
| Multiplex Fluorescent Detection Kit v2 | Advanced Cell Diagnostics (ACD) | Cat# 323110 |
| RNeasy Plus Micro Kit | Qiagen | Cat# 74034 |
| High-Capacity cDNA Reverse Transcription Kit | ThermoFisher | Cat# 4368814 |
| RNAqueous-Micro Total RNA Isolation Kit | ThermoFisher | Cat# AM1931 |
| SMARTer Stranded Total RNA-seq kit v2 - Pico Input | TaKaRa Bioscience | Cat# 634412 |
| KAPA HIFI HotStart ReadyMix PCR kit | Roche Diagnostics | Cat# 07958935001 |
| AMPure XP | Beckman Coulter | Cat# A63880 |
| **Deposited data** | | |
| Single-cell RNA sequencing of human Fallopian tube WβS-reporter organoids | This study | GEO: GSE239582 |
| Bulk RNA sequencing of human Fallopian tube WβS-reporter organoids | This study | GEO: GSE239581 |
| Single Cell RNA sequencing of patient-derived fibroblast and immune cells | Hu et al. (2020)[10] | GEO: GSE132149 |
| Single-cell RNA sequencing of patient-derived Fallopian tube cells | Hu et al. (2020)[10] | GEO: GSE132149 |
| **Experimental models: Cell lines** | | |
| Human Fallopian tube organoid lines | This study (available upon request) | N/A |

(*Continued on next page*)

*Continued*

| REAGENT or RESOURCE | SOURCE | IDENTIFIER |
|---|---|---|
| Human Fallopian tube WβS-reporter organoid lines | This study (available upon request) | N/A |
| Mouse oviduct organoid lines | This study (available upon request) | N/A |
| Mouse oviduct WβS-reporter organoid lines | This study (available upon request) | N/A |
| HEK293 cells | ATCC | Cat# CRL-1573 |
| L-WNT3A cell line | ATCC | Cat# CRL-2647 |
| HA-R-Spondin1-Fc 293T cell line | AMSbio | Cat# 3710-001-01 |
| **Experimental models: Organisms/strains** | | |
| Female mice, strain C57BL/6, aged 7–12 weeks | Biomedical Sciences Facility, University of Oxford | N/A |
| **Oligonucleotides** | | |
| Probe (3-plex human Positive Control) | Bio-Techne | Cat# 320861 |
| Probe (3-plex mouse Positive Control) | Bio-Techne | Cat# 320881 |
| Probe (3-plex Negative Control) | Bio-Techne | Cat# 320871 |
| Probe (human WNT7A) | Bio-Techne | Cat# 408231 |
| Probe (human AXIN2) | Bio-Techne | Cat# 400241-C2 |
| Probe (human LGR5) | Bio-Techne | Cat# 311021-C3 |
| Probe (mouse Wnt7a) | Bio-Techne | Cat# 401121 |
| Probe (mouse Axin2) | Bio-Techne | Cat# 400331-C2 |
| Probe (mouse Lgr5) | Bio-Techne | Cat# 312171-C3 |
| Non-targeting siRNA | Dharmacon | Cat# D-001210-05-20 |
| β-catenin (*CTNNB1*) siRNA_09 | Dharmacon | Cat# J-003482-09 |
| β-catenin (*CTNNB1*) siRNA_10 | Dharmacon | Cat# J-003482-10 |
| β-catenin (*CTNNB1*) siRNA_11 | Dharmacon | Cat# J-003482-11 |
| β-catenin (*CTNNB1*) siRNA_12 | Dharmacon | Cat# J-003482-12 |
| Non-Targeting (SMARTpool) siRNA | Dharmacon | Cat# D-001206-13-05 |
| *WNT7A* siRNA | Dharmacon | Cat# M-008543-01-0005 |
| *FZD3* siRNA | Dharmacon | Cat# L-005502-00-0005 |
| *FZD5* siRNA | Dharmacon | Cat# L-005504-00-0005 |
| *FZD6* siRNA | Dharmacon | Cat# L-005505-00-0005 |
| qPCR primer sequences | see Table S5 | N/A |
| **Recombinant DNA** | | |
| 7TGC (WNT signaling reporter plasmid) | Fuerer & Nusse, 2010[24] | Addgene Cat# 24304 |
| pMD2.G (VSV-G envelope plasmid) | Gift from Didier Trono (unpublished) | Addgene Cat# 12259 |
| psPAX2 (lentiviral packaging plasmid) | Gift from Didier Trono (unpublished) | Addgene Cat# 12260 |
| M50 Super 8x TOPFlash | Veeman et al., 2003[88] | Addgene Cat# 12456 |
| pcDNA.Control | ThermoFisher | Cat# 12489019 |
| pcDNA.WNT7A | Najdi et al., 2012[89] | Addgene Cat# 35914 |
| pcDNA.WNT7A-V5 | MacDonald et al., 2014[90] | Addgene Cat# 43816 |
| pcDNA.WNT3A | Najdi et al., 2012[89] | Addgene Cat# 35908 |
| pRK5-mFzd3-1D4 plasmid | Yu et al., 2012[33] | Addgene Cat# 42265 |
| pRK5-mFzd5-1D4 plasmid | Yu et al., 2012[33] | Addgene Cat# 42267 |
| pRK5-mFzd6-1D4 plasmid | Yu et al., 2012[33] | Addgene Cat# 42268 |
| pCMV-hERα plasmid | Mao et al., 2008[91] | Addgene Cat# 101141 |
| pcDNA3-PRβ plasmid | Su et al., 2012[92] | Addgene Cat# 89130 |
| **Software and algorithms** | | |
| ZEN 3.0 image analysis software | Zeiss | https://www.zeiss.com/microscopy/en/products/software/zeiss-zen.html |

(*Continued on next page*)

*Continued*

| REAGENT or RESOURCE | SOURCE | IDENTIFIER |
|---|---|---|
| Prism v8/9 | GraphPad software | https://www.graphpad.com/scientific-software/prism/ |
| R Statistical Software (v4.1.1) | R Project for Statistical Computing | https://www.R-project.org/ RRID: SCR_001905 |
| Seurat (v4.3.0) | Hao et al. (2021)[93] | https://satijalab.org/seurat/ RRID:SCR_016341 |
| edgeR (v3.36.0) | Robinson et al. (2010)[94] | https://bioconductor.org/packages/3.14/bioc/html/edgeR.html RRID:SCR_012802 |
| MSigDB (v2022.1.Hs) | Subramanian et al. (2005)[95] | https://www.gsea-msigdb.org/gsea/msigdb/index.jsp RRID:SCR_016863 |
| fgsea (v1.20.0) | Sergushichev (2016)[96] | https://bioconductor.org/packages/3.14/bioc/html/fgsea.html RRID:SCR_020938 |
| STAR (v2.7.3a) | Dobin et al. (2013)[97] | https://github.com/alexdobin/STAR |
| FeatureCounts (v2.0.0) | Liao et al. (2014)[98] | https://github.com/ShiLab-Bioinformatics/subread |
| ToppFun | Chen et al. (2009)[99] | https://toppgene.cchmc.org/enrichment.jsp |
| Other | | |
| ACD HybEZ™ II Hybridization System | Bio-Techne | Cat# 321720 |

## RESOURCE AVAILABILITY

### Lead contact

Further information and requests for resources should be directed to and will be fulfilled by the lead contact, Ahmed Ahmed (ahmed.ahmed@wrh.ox.ac.uk).

### Materials availability

This study did not generate new unique reagents.

### Data and code availability

- The RNA-Seq data generated in this study are available at NCBI GEO under the following accession numbers and are publicly available as of the date of publication: Single-cell RNA sequencing of human Fallopian tube WβS-reporter organoids (GEO: GSE239582); Bulk RNA sequencing of human Fallopian tube WβS-reporter organoids (GEO: GSE239581). This paper analyses existing publicly available single cell-RNA sequencing datasets of patient-derived Fallopian tube cells (GEO: GSE132149) and patient-derived fibroblast and immune cells (GEO: GSE132149). These are published.[10]
- This paper does not report original code.
- Any additional information required to reanalyse the data reported in this paper is available from the lead contact upon request.

## EXPERIMENTAL MODEL AND STUDY PARTICIPANT DETAILS

### Human subjects and tissue Acquisition

Fallopian tube tissue samples were obtained from patients undergoing cancer surgery at the Department of Gynecological Oncology, Churchill Hospital, Oxford University Hospitals, United Kingdom. Patients were appropriately informed and consented in writing, and cases were recruited as part of the Gynecological Oncology Targeted Therapy Study 01 (GO-Target-01, Research Ethics Approval #11-SC-0014, Berkshire NRES Committee), as well as under the Oxford Center for Histopathology Research (OCHRe)/Oxford Radcliffe Biobank (ORB) research tissue bank ethics ref. 19/SC/0173. Detailed patient and clinical information can be found in Table S1. The experiments conducted in this manuscript were part of a discovery pilot research project on human samples. Therefore, no formal sample size calculation or group assignment estimation were performed. Unless otherwise stated, all experiments were conducted at least in triplicates to ensure reproducibility and to estimate heterogeneity.

### Mouse tissue Acquisition

All mouse tissue samples were harvested and provided by the Biomedical Sciences Facility, University of Oxford. Mouse colonies were maintained in certified and licensed animal facilities and in accordance with the United Kingdom's Home Office Animals (Scientific Procedures) Act 1986. All personnel handling animals held Home Office-issued Personal Licenses. Tissues were obtained from female mice, strain C57BL/6 and aged 7–12 weeks.

## METHOD DETAILS

### Tissue dissociation & primary Culture

Human or mouse tissue was washed, cut longitudinally to expose the epithelium and dissociated in pre-warmed Digestion medium containing Trypsin (2 mg/mL, Sigma), DNase I (0.5 mg/mL, Sigma) and Collagenase Type I (100 U/ml, Invitrogen) for 45 min to 1 h at 37°C in constant rotation. Cells were passed through a 70, 100 or 250 μm cell strainer and pelleted by centrifugation at 300*g*/5 min/4°C, washed with cold DPBS and used for downstream analysis. For primary 2D culture, isolated cells were resuspended in BM2 culture medium containing Advanced DMEM/F12 (ThermoFisher), HEPES (12 mM, ThermoFisher), FBS (5%, GIBCO), Penicillin/Streptomycin (1%, GIBCO), EGF (100 ng/mL, ThermoFisher) and Y-27632 ROCK inhibitor (10 μM, Sigma), as described.[9] For Western blot, primary FT 2D culture was expanded in 6-well plates and treated as described. For siRNA knockdown, 40 nM of siRNA was transfected for 72–96 h using Lipofectamine 3000 (ThermoFisher Scientific) according to the manufacturer's protocol.

### Human Fallopian tube Organoid Culture

To establish human FT organoids, processed cell pellets from dissociated FT tissue were resuspended in Extracellular Matrix (ECM, Matrigel, Corning), plated as 50 μL drops on pre-warmed culture plates and incubated at 37°C for 20-30 min to allow Matrigel polymerization. Cells were then overlaid with pre-warmed Organoid Medium containing BM2 medium above (without FBS), supplemented with Noggin (100 ng/mL, Peprotech), Fibroblast Growth Factor 10 (100 ng/mL, Peprotech), N2 supplement (1%, ThermoFisher), B27 supplement (2%, ThermoFisher), Nicotinamide (1 mM, Sigma), N-acetyl L-cysteine (1 mM, Sigma), A83-01 (5 μM, StemCell Technologies), Forskolin (10 μM, Bio-Techne) and R-Spondin 1 (500 ng/mL, in-house produced or Peprotech) at the indicated concentrations. Surrogate Wnt (0.5 nM, ImmunoPrecise) was used wherever indicated. Y-27632 (10 μM) was added for the first 2–3 days of organoid culture. WNT3A conditioned medium was generated in-house using L-WNT3A cells (ATCC) or by transient transfection of pcDNA.WNT3A (gift from Marian Waterman) into HEK293 cells (see below).

For maintenance of hFT organoids, organoids were passaged at a ratio of 1:3 to 1:5 every 10–14 days. Briefly, organoids were released from Matrigel by incubation with Organoid Harvesting Solution (Culturex) at 4°C in rotation, for 45–90 min. Organoids were then collected into a 15 mL or 50 mL falcon tube, pelleted by centrifugation at 300*g*/10 min/4°C, washed with cold PBS once and used for passage or FACS-related downstream analysis. For passage, the organoid pellet was dissociated by mechanically shearing organoids using a p200 pipette. For flow analysis or FACS sorting, single cell dissociation was performed by resuspending organoids in pre-warmed 7.5X TrypLE Express (ThermoFisher) diluted in Organoid Wash Buffer (OWB), for 5–10 min. OWB buffer is composed of complete organoid medium + Y26632 but lacking growth factors (EGF, FGF-10, Noggin and RSPO1). Organoids (now single cells) were then washed twice with cold PBS and utilized for FACS or single cell culture. For cryopreservation, pelleted organoids were mechanically fragmented as described, embedded in Recovery Cell Culture Freezing Medium (ThermoFisher), transferred to −80°C freezer overnight and finally transferred to Liquid Nitrogen for long-term storage. For culture re-establishment after cryopreservation, thawed organoids were resuspended in 9 mL OWB buffer, pelleted, washed and cultured in a well of a 24-well plate, as described.

### Mouse oviduct Organoid Culture

Mouse oviduct organoids were established from primary tissue as described above for hFT organoids. Culture medium for mouse organoids was the same as hFT organoids, excluding A83.01 and Forskolin. Mouse organoids were passaged as reported.[3]

### Organoid formation efficiency (OFE) assay

OFE analysis was performed on single cell dissociated tissue or organoids, derived as described above. After quantifying cell number, cells were resuspended in Matrigel and plated as 50 μL drops in 24-well plates or 7 μL drops in 48 or 96-well plates. Organoids were treated with CHIR99021 (3 μM, Bio-Techne), IWP-2 (2 μM, Bio-Techne), LGK-974 (2 μM, Stratech Scientific), XAV-939 (5 μM, Stratech Scientific), PRI-724 (10 μM, Abcam), Surrogate Wnt (0.5 nM, ImmunoPrecise), IgG-2919/IgG-2921 (Sidhu Lab, 0.5 μM), Valproic acid (1 mM, Bio-Techne), DAPT (10 μM, Bio-Techne), Estrogen (100 nM, Bio-Techne), Progesterone (1 μM, Bio-Techne) or/and recombinant human WNT7A protein (500 ng/mL, R&D), as indicated in the text. Unless otherwise stated, treatments were started on plating day for 7–12 days. OFE was estimated as the % of the number of cells forming organoids out of the total cell number plated. For experiments requiring FACS isolation, cells were prepared for FACS by cold PBS washing followed by blocking non-specific antibody staining using human or mouse FcR Blocking Reagent (Miltenyi Biotech, 1:10) for 10 min in the dark in a fridge. Further antibody incubation was performed using human CD45-FTIC (1:50, Biolegend) and human EpCAM-APC (1:10, Miltenyi Biotech), or mouse CD45-FTIC (1:50, Miltenyi Biotech) and mouse EpCAM-APC (1:10, Miltenyi Biotech), in a total volume of 100 μL volume. WβS-reporter organoids (see below) were FACS isolated using mCherry gating, and non-transduced parental organoid lines were used as negative controls. FACS-isolated cells were sorted directly into Matrigel, cultured for 10–14 days and OFE quantified as described.

### Generation of WβS-reporter organoids

To generate WβS-reporter organoids, viral lenti-particles were generated by transfecting HEK293 cells in a T25 flask with 15 μg of the lentiviral WβS-reporter vector (7TGC; gift from Roel Nusse[24]; see Figure 2A for map) and 15 μg of each of the viral envelope (pMD2.G) and packaging (psPAX2) plasmids, both gifts from Didier Trono. Transfections were performed using the Lipofectamine 3000 protocol (ThermoFisher). Viral supernatant was concentrated using the Lenti-X Concentrator (Takara). Primary 2D-cultured FT cells were transduced at p.0 in BM2 medium (see above) containing Polybrene (8 μg/mL, Sigma), for 72 h. Transduced cells were selected by FACS and sorted directly into Matrigel. Organoid culture was established and expanded from transduced cells and passaged/expanded as described above. WβS-reporter organoids can be made available upon request.

### scRNA-seq of WβS-reporter organoids

Single cell RNA sequencing (scRNA-seq) was performed on low passage hFT WβS-reporter organoid lines. Organoids were harvested on days 8–11 as described above. RNasin Plus RNase inhibitor (Promega) was included at the harvesting and dissociation steps, to protect RNA integrity while organoids are recovered. Organoids (now single cells) were resuspended in OWB buffer containing RNase inhibitor, 2 mM EDTA and 1% RNase-free BSA (Sigma). Cells were passed through a 30 μm cell strainer and single cell FACS sorting performed using the MA900 Sony Sorter. Isolated WNT/β-catenin Signaling Active (WβA) cells or non-WβA cells were sorted into 96-well plates containing 4 μL lysis buffer supplemented with 0.1 μL RNase inhibitor (Clonetech), 1.9 μL 0.4% Triton X-100, 1 μL 10 μM 5'-biotinylated oligo-dT30VN (IDT) and 1 μL 10 mM dNTP (Thermo Scientific). Cells were sorted at one cell per well, with bulk controls (10 cells) and empty well controls (0 cells) included for each plate. Plates were snap frozen on dry ice and stored at - 80°C for less than 4 weeks.

Single cell cDNA synthesis and library generation were performed according to the SMART-seq2 protocol,[26] as previously described.[10] Briefly, cells were lysed by removing plates from −80°C and heating at 72°C for 3 min. Plates were then placed at 4°C before adding the reverse transcription mix containing 5'-biotinylated TSO (Qiagen). PCR products were cleaned up using 0.8:1 Ampure XP beads (Beckman Coulter) with Biomek FxP Laboratory Automation Workstation (Biomek). Quality of single-cell cDNA was tested using TapeStation, as well as by single cell qPCR for GAPDH or ACTB using the QuantiNova SYBR Green PCR Kit (Qiagen). cDNA concentration was measured using Quant-iT PicoGreen dsDNA Assay Kit (Invitrogen) on the CLARIOstar Plate Reader (BMG Labtech). Wells with $C_T$ values of GAPDH or ACTB below 20 were selected as wells with good quality cDNA. Libraries from single cell cDNA were generated using miniaturized Nextera XT (Illumina) protocol[100] with Mosquito HTS (TTP LabTech), in 384-well Endure plate (Life Technology). Library sequencing was performed by Novogene.

### Bulk RNA-seq of WβS-reporter organoids

hFT WβS-reporter organoids were generated and dissociated as described above. WβA or non-WβA cells were FACS-isolated and sorted directly into RNA lysis buffer. RNA extraction and DNase digestion were performed using the RNAqueous-Micro Total RNA Isolation Kit (Thermo Fisher Scientific) according to the manufacturer's protocol. RNA integrity was evaluated using the 2200 TapeStation system (Agilent). The SMARTer Stranded Total RNA-seq kit v2 - Pico Input (Takara) was used to prepare sequencing libraries, which were then assessed with TapeStation (Agilent) and quantified by Qubit (Thermo Fisher Scientific). Library sequencing was performed by Novogene.

### Organoid RNA extraction & RT-qPCR

For RNA extraction, organoids were harvested as described above. Matrigel was solubilized and washed away using the Organoid Harvesting Solution (Bio-Techne) and cold DPBS. Pelleted organoids were mechanically fragmented in cold DPBS, pelleted, resuspended in 350 μL RLT buffer (Qiagen) and transferred into a 1.5 mL Eppendorf tube. The tube was incubated for 15 min at room temperature in rotation and then vortexed for 1 min. RNA extraction was performed according to the Qiagen RNeasy Plus Micro Kit. Extracted RNA was tested for concentration (using NanoDrop) and, if required, for quality (using TapeStation). Up to 2 μg of extracted RNA was used to generate cDNA using the High Capacity cDNA Reverse Transcription Kit (Applied Biosystems). RT-qPCR was set up using the SYBR Green PCR Master Mix (ThermoFisher) and conducted using the StepOnePlus RT-PCR machine (ThermoFisher). All data was normalized to endogenous controls *GAPDH* (human) or *Hprt* (mouse), and fold change was quantified by normalization to untreated samples. All qPCR primer sequences were obtained from Sigma. Primer sequences are shown below and unless otherwise stated, all primers target human genes.

AXIN2 (F): 5′-AGTGTGAGGTCCACGGAAAC-3′ AXIN2 (R): 5′-CTGGTGCAAAGACATAGCCA-3′
Axin2 (mouse, F): 5′-TGTCCAGCAAAACTCTTC-3′ Axin2 (mouse, R): 5′-CTTCTCTTGAAGGACCTGA-3′
BRCA1 (F): 5′-GAAACCGTGCCAAAAGACTTC-3′ BRCA1 (R): 5′-CCAAGGTTAGAGAGTTGGACAC-3′
BRCA2 (F): 5′-TGCCTGAAAACCAGATGACTATC-3′ BRCA2 (R): 5′-AGGCCAGCAAACTTCCGTTTA-3′

*CAPS (F): 5′-AGGGTGTGTGCAGGAAGTG-3′ CAPS (R): 5′-GGTCCAGCTTGGCAAATG-3′*

*CCDC17 (F): 5′-TGTGGGACCTGTGACATGGT-3′ CCDC17 (R): 5′-ACGCCCTGGTGTTCTTGTG-3′*

*CCDC78 (F): 5′-AATGTTGTGCTACGAGCCAAG-3′ CCDC78 (R): 5′-CTGGGGTCAGACTCCACTG-3′*

(*Continued on next page*)

| Continued |
| --- |
| CAPS (F): 5′-AGGGTGTGTGCAGGAAGTG-3′ CAPS (R): 5′-GGTCCAGCTTGGCAAATG-3′ |
| CTNNB1 (F): 5′-AAAGCGGCTGTTAGTCACTGG-3′ CTNNB1 (R): 5′-CGAGTCATTGCATACTGTCCAT-3′ |
| EGFP (F): 5′-AAGGGCATCGACTTCAAGG-3′ EGFP (R): 5′-TGCTTGTCGGCCATGATATAG-3′ |
| ESR1 (F): 5′-CCCACTCAACAGCGTGTCTC-3′ ESR1 (R): 5′-CGTCGATTATCTGAATTTGGCCT-3′ |
| FOXJ1 (F): 5′-CAACTTCTGCTACTTCCGCC-3′ FOXJ1 (R): 5′-CGAGGCACTTTGATGAAGC-3′ |
| FZD3_1 (F): 5′-AATATGGACGTGTCACACTTCC-3′ FZD3_1 (R): 5′-GGATATGGCTCATCACAATCTGG-3′ |
| FZD3_2 (F): 5′-GTTCATGGGGCATATAGGTGG-3′ FZD3_2 (R): 5′-GCTGCTGTCTGTTGGTCATAA-3′ |
| FZD5_1 (F): 5′-CATGCCCAACCAGTTCAACC-3′ FZD5_1 (R): 5′-CGGCGAGCATTGGATCTCC-3′ |
| FZD5_2 (F): 5′-CCGTTCGTGTGCAAGTGTC-3′ FZD5_2 (R): 5′-GAAGCGTTCCATGTCGATGAG-3′ |
| FZD6_1 (F): 5′-ATGGCCTACAACATGACGTTT-3′ FZD6_1 (R): 5′-GTTTACGACAAGGTGGAACCA-3′ |
| FZD6_2 (F): 5′-GAGCAAGTGAACAGGATTACCT-3′ FZD6_2 (R): 5′-ATTCTGGTCGAGCTTTTGC-3′ |
| GAPDH (F): 5′-GCAAATTCCATGGCACCG-3′ GAPDH (R): 5′-TCGCCCCACTTGATTTTGG-3′ |
| HES1 (F): 5′-ACGTGCGAGGGCGTTAATAC -3′ HES1 (R): 5′-GGGGTAGGTCATGGCATTGA-3′ |
| HES7 (F): 5′-CGGGATCGAGCTGAGAATAGG-3′ HES7 (R): 5′-GCGAACTCCAATATCTCCGCTT-3′ |
| Hprt (mouse, F): 5′-AAGTTTGTTGTTGGATATGC-3′ Hprt (mouse, R): 5′-CATCTTAGGCTTTGTATTTGG-3′ |
| KI-67 (F): 5′-CCTGTACGGCTAAAACATGGA-3′ KI-67 (R): 5′-GCTGGCTCCTGTTCACGTA-3′ |
| Krt5 (mouse, F): 5′-TCTGCCATCACCCCATCTGT-3′ Krt5 (mouse, R): 5′-CCTCCGCCAGAACTGTAGGA-3′ |
| LGR5 (F): 5′-CAGCGTCTTCACCTCCTACC-3′ LGR5 (R): 5′-GTTTCCCGCAAGACGTAACT-3′ |
| LGR6 (F): 5′-GCCTGAAAATCCTGATGCTG-3′ LGR6 (R): 5′-ACCAGGGAGATGAGGTTGG-3′ |
| MYBL2 (F): 5′-GGTGGCTGAGAGTTTTGAATCC-3′ MYBL2 (R): 5′-CCTCCTCGGTCCAGCAAGA-3′ |
| PAX8 (F): 5′-TGCCTCACAACTCCATCAGA-3′ PAX8 (R): 5′-CAGGTCTACGATGCGCTG-3′ |
| PGR (F): 5′-TTATGGTGTCCTTACCTGTGGG-3′ PGR (R): 5′-GCGGATTTTATCAACGATGCAG-3′ |
| TFF1 (F): 5′-CCCCGTGAAAGACAGAATTGT-3′ TFF1 (R): 5′-GGTGTCGTCGAAACAGCAG-3′ |
| WNT7A_1 (F): 5′-TGCCCGGACTCTCATGAAC-3′ WNT7A_1 (R): 5′-GTGTGGTCCAGCACGTCTTG-3′ |
| WNT7A_2 (F): 5′-CTGTGGCTGCGACAAAGAGAA-3′ WNT7A_2 (R): 5′-GCCGTGGCACTTACATTCC-3′ |
| WNT7A_3 (F): 5′-GGGACTATGAACCGGAAAGC-3′ WNT7A_3 (R): 5′-GGCCTGGGATCTTGTTACAG-3′ |

### RNA In situ Hybridization (RNAScope)

A small piece of primary human or mouse tissue was resected and embedded in Fisher Healthcare Tissue-Plus Optimum Cutting Temperature (OCT, ThermoFisher). This was frozen at −80°C, sectioned into 10 μm sections using the CryoStar NX50 (Thermo Scientific) cryostat, mounted on regular glass slides (SuperFrost Plus, VWR International) and immediately stored at - 80°C. RNA *In situ* Hybridization was performed using the RNAScope Multiplex Fluorescent v2 kit (ACD) as described[101] for fresh frozen human or mouse tissue. Organoid sections were established by dissociating organoids, washing and attaching dissociated cells to a slide by Cytospining (FisherScientific) according to the manufacturer's protocol. Slides were immediately fixed in 4% PFA. RNA FISH staining was performed as per the RNAScope protocol (ACD).

### Organoid Immunofluorescence staining

Organoids were prepared for antibody staining by culture for 7–12 days on an 8-well microscopy chamber slide (Thistle Scientific) followed by whole-mount staining within Matrigel. Briefly, organoids were washed with PBS and fixed for 15–20 min using 2% Paraformaldehyde diluted in DPBS (ThermoFisher). To reduce background staining, samples were washed three times (10 min each) with PBS containing 0.4M Glycine (Sigma). Permeabilization was performed for 10 min using 0.5% Triton X-100 in PBS. All washing, blocking and antibody staining steps were performed in wash buffer containing 0.2% Triton X-100 and 0.05% Tween 20 in PBS. Blocking was done in 5–10% Normal Donkey Serum (Sigma) for 2–3 h. Primary antibody incubation was performed overnight at 4°C in motion using one or more of the following antibodies at the indicated dilutions: E-cadherin (1:200, BD Biosciences), Ki-67 (1:100, Cell Signaling), PAX8 (1:50, Proteintech), TUBB4 (1:100, Sigma), pan cytokeratin (1:250, Abcam) or c-Myc (1:100, Cell Signaling). Secondary antibody incubation was done for 2–3 h at room temperature. Samples were mounted in Vectashield Mounting Medium (Vector Laboratories). Images were obtained using the Zeiss LSM 780 Inverted Confocal Microscope.

### Wnt-reporter/TOPFlash assay

All plasmids, small molecule inhibitors or expressed proteins that modulate the WβS pathway were functionally validated using the TOPFlash assay. In brief, 100K–200K HEK293 cells were reverse transfected with the M50 Super 8x TOPFlash plasmid[88] (100 ng; gift from Randall Moon) and Renilla luciferase construct (5 ng, Merck Millipore) in 24-well plates for 48–72 h. After that, WβS pathway

modulators were introduced at the desired concentrations in fresh medium and incubated overnight. Next day, lysates and luciferase reaction substrates were prepared using the Dual-Luciferase Reporter Assay System (Promega) according to the manufacturer's protocol, and luciferase readings were acquired using the automated dual injector GloMax Luminometer (Promega). Relative WβS levels were estimated by normalizing Firefly luciferase to Renilla luciferase readings and normalizing this quotient to the Unt sample. Depending on the experimental set up, one or more plasmids (see key resources table) or siRNA's (see below) were co-transfected with the above as indicated in the text. For all TOPFlash assays, plasmids were used at 200 ng per well and siRNAs at 40nM, unless otherwise stated. For hormone stimulation experiments, estrogen (17β-estradiol, also called E2, 100 nM) or/and progesterone (P4, 1 μM) were used at the indicated concentrations for 24 h.

Sequences of siRNA's used in TOPFlash assays were as shown below. All siRNAs were obtained from Dharmacon (Horizon Discovery). siRNA source and catalog/identifiers can be found in the key resources table: Non-targeting siRNA (5′-UGG UUU ACA UGU CGA CUA A-3′); β-catenin siRNA_09 (5′-GAU CCU AGC UAU CGU UCU U-3′), β-catenin siRNA_10 (5′-UAA UGA GGA CCU AUA CUU A-3′); β-catenin siRNA_11 (5′-GCG UUU GGC UGA ACC AUC A-3′); β-catenin siRNA_12 (5′-GGU ACG AGC UGC UAU GUU C-3′); Non-targeting SMARTpool siRNA (5′-UAG CGA CUA AAC ACA UCA A-3′, 5′-UAA GGC UAU GAA GAG AUA C-3′, 5′-AUG UAU UGG CCU GUA UUA G-3′, 5′-AUG AAC GUG AAU UGC UCA A-3′); FZD3 SMARTpool siRNA (5′-CCA AAU ACU CCU AUC AUA A-3′, 5′-ACA GAU CAC UCC AGG CAU A-3′, 5′-GUU CGA AGC UCA UGG AGA U-3′, 5′-UGA UUG AUG UCA CAA GAU U-3′); FZD5 SMARTpool siRNA (5′-GCA UGU GGU GGC CUG CUA-3′, 5′-GCA CAU GCC CAA CCA GUU C-3′, 5′-AAA UCA CGG UGC CCA UGU G-3′, 5′-GAU CCG CAU CGG CAU CUU C-3′); FZD6 SMARTpool siRNA (5′-CCA GAG AGA CCA AUU AUA U-3′, 5′-UCG CAA AUC UGG AAU GUU C-3′, 5′-GAA GGA AGG AUU AGU CCA A-3′, 5′-CAG UGA AAG UCG AAG AGU A-3′).

### Cell Culture, protein expression & Western blotting

RSPO1 protein expression and isolation was performed using the HEK293T HA-R-Spondin1-Fc cell line, according to the manufacturer's protocol (Culturex). WNT3A protein expression was performed using the L-WNT3A cell line according to the manufacturer's protocol (ATCC). WNT7A protein was expressed by transfecting the pcDNA.WNT7A[89] (gift from Marian Waterman), pcDNA.WNT7A-V5[90] (gift from Xi He) or empty control plasmid into HEK293 cells and harvesting the conditioned medium after 96 h. For siRNA knockdown, WNT7A SMARTpool siRNA was used (5′-GCG CAA GCA UCA UCU GUA A-3′, 5′-UCA AGA AGC CAC UGU CGU A-3′, 5′-CAA CGA GGC AGG CCG AAA G-3′, 5′-GAA CUG CUC UGC ACU GGG A-3′). Non-targeting SMARTpool siRNA (see above for sequence) was used as control. Both siRNAs were obtained from Dharmacon (Horizon Discovery). siRNA source and catalog/identifiers can be found in the key resources table. For investigating the effect of estrogen and progesterone on WNT7A protein, 800K HEK293 cells were transfected in 6-well plates for 96 h with 1 μg of the pcDNA.WNT7A, pCMV-hERα[91] or/and pcDNA3-PRβ[92] plasmids (ERα and PRβ plasmids were gifts from Elizabeth Wilson) in the combinations indicated in the text. Estrogen (17β-estradiol, also called E2, 100 nM) or/and progesterone (P4, 1 μM) were introduced on transfection day for 96 h at the indicated concentrations. Western blot was performed on cell lysates and harvest conditioned medium. For Western blotting figures, the following antibodies were used at the indicated dilutions: WNT7A (1:800, Abcam), active β-catenin (1:1,000, Merck Millipore), V5 tag (1:500, Abcam) and GAPDH (1:1,000, Proteintech). Secondary antibodies used were IRDye 800CW goat anti-rabbit IgG (1:10,000, LI-COR) or/and IRDye 680RD goat anti-mouse IgG (1:10,000, LI-COR).

## QUANTIFICATION AND STATISTICAL ANALYSIS

### Single Cell RNA-seq analysis

scRNA-seq analysis was performed using R (v4.1.1) and Seurat (v4.3.0) packages.[93] Genes detected in <3 cells, cells with UMI counts <10,000 and gene counts <200 were removed, resulting in the detection of 16,969 genes in 1,021 cells across a total of 3 patient-derived WβS-reporter organoids, with a median of ~340 cells from each sample. Raw counts were normalized using the LogNormalize method and ScaleData function with multiple regression variables, including nCount_RNA, S.Score, and G2M.Score. Cells were then clustered using K-nearest neighbor (KNN) graphs and the Louvain algorithm using the first 30 dimensions from principal component analysis. Clustered cells were visualized by UMAP embedding using the default settings. For each sample, differential expression analysis was performed comparing WβA and non-WβA cells using edgeR v3.36.0.[94] Only features detected in >10% of either cell type using FindMarkers were included. Gene expression signatures were derived by identifying genes that exhibited consistent expression level differences, with p value <0.05, across the 3 samples. Gene set enrichment analysis (GSEA[95,102]) was performed using the fgsea package (v1.20.0)[96] and MSigDB collections (v2022.1.Hs). Pathways that were upregulated or downregulated in WβA cells relative to non-WβA cells (fdr-adjusted $p < 0.25$) in all samples were selected.

### Bulk RNA-seq analysis

For bulk RNA-seq, sequencing reads from FASTQ files were trimmed for adapter sequences and quality with Trim Galore! and mapped to the UCSC hg19 human genome assembly using STAR (v2.7.3a).[97] Read counts were obtained using subread FeatureCounts (v2.0.0).[98] For differential expression analysis, this was performed using edgeR (v3.36.0) with cut-offs of $p < 0.05$ and FDR <0.05. When the analysis was repeated by relaxing the FDR to 0.1, the same list of DEGs was obtained. Pathway analysis was performing using ToppFun.[99]